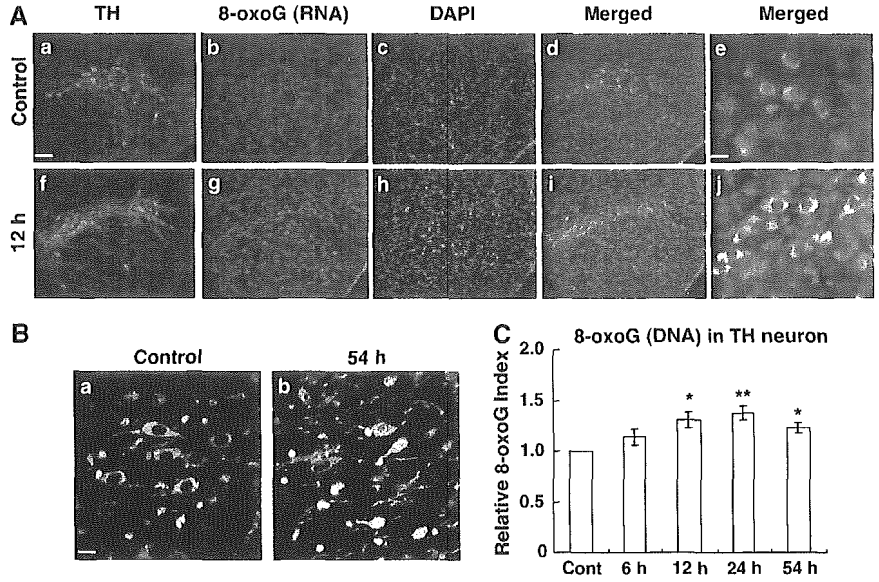

Figure 3 *Increased accumulation of 8-oxoG in the nuclear DNA and cellular RNA of dopamine neurons in the substantia nigra after MPTP administration.* Animals were treated as in Figure 2A. (**A**) The localization of 8-oxoG in cellular RNA of the dopamine neurons in the SN determined by fluorescence microscopy. The sections stained for TH (a, f), 8-oxoG in RNA (b, g), and nuclear DNA with DAPI (c, h) are shown. The merged images (d, i); their magnification (e, j). Control (a–e); 12 h after the first MPTP injection (f–j). Scale bars (a–d, f–i), 100 μm (e, j), 20 μm. (**B**) The localization of 8-oxoG in nuclear DNA of the dopamine neurons in the SNc determined by laser scanning confocal microscopy. The sections were stained for TH (red) and 8-oxoG in nuclear DNA (green), and their merged images are shown. Control (a); 54 h after the first MPTP injection (b). The nuclear localization of 8-oxoG in the TH-positive neurons was evident after MPTP administration. Scale bar: 10 μm. (**C**) The increased accumulation of 8-oxoG in nuclear DNA in the TH-positive dopamine neurons in the SNc after MPTP administration. The immunoreactivities for 8-oxoG in each TH-positive cell were separately digitized from the data shown in Figure 3B, and the 8-oxoG index in each sample was determined. The relative value of each 8-oxoG index to that of the control is shown with the means $\pm$ S.D. ($n = 4$ per group). Mann–Whitney *U*-test, $^{**}P < 0.02$, $^{*}P < 0.05$ compared to the control

observed (Figure 4Ff). Simultaneously, 8-oxoG immunoreactivitiy in the striatum with RNase pretreatment but not HCl pretreatment also apparently increased to more than 130% level of the control (Figure 4M, N, m, n), and thereafter decreased (Figure 4O, P, o, p). At 24 h after the first injection, the terminal dysfunction of dopamine neurons in the NAc and olfactory tubercle (OT) became apparent as well as in the striatum (Figure 4C), and GFAP immunoreactivitiy also increased (Figure 4I–K, i–k), thus indicating that astrocytes were activated in the striatum. Next, 54 h later with three MPTP injections, the terminal dysfunction of dopamine neurons in the striatum, nucleus accumbenes (NAc) and OT was highly prominent (Figure 4D), and accompanied with more activated astrocytes (Figure 4L, l).

As a result, we concluded that the oxidative damage in the nucleic acids of nigrostriatal dopamine neurons is transiently increased during MPTP-induced PD mouse model.

Expression of *Mth1* mRNA encoding an oxidized purine nucleoside triphosphatase in normal mouse brain

We recently showed the accumulation of 8-oxo-dGTP and/or 2-OH-dATP in cellular nucleotide pools to cause cell death, while MTH1 hydrolyzing these oxidized nucleotides to monophosphates efficiently suppresses such cell death.[14] In order to examine the role of MTH1 for neuroprotection in damaged brain, we next analyzed the expression of *Mth1* mRNA in mouse brain by *in situ* hybridization. Antisense but not sense probe for *Mth1* mRNA exhibited positive signals in neurons throughout brain (Figure 5Aa, b). Neurons in the SN including SNc, SNr and ventral tegmental area (VTA) exhibited substantial levels of *Mth1* mRNA expression (Figure 5Ba–c), as well as neurons in the cerebral cortex and hippocampus (Figure 5Bd–f). The expression of *Mth1* mRNA in the brain was confirmed by RT-PCR (data not shown).

A Western blotting analysis revealed the definite expression of MTH1 protein in the striatum of the control and MPTP-treated wild-type mice, and no detectable MTH1 protein in the striatum of either control or MPTP-treated MTH1-null mice (Figure 5C). The expression level of MTH1 protein in the striatum of wild-type mice apparently decreased after MPTP treatment, probably due to the terminal loss of dopamine neurons (Figure 5C, lane 3).

Dopamine neuron loss in SNc induced by MPTP was not affected by MTH1 deficiency

Given the observed increase of 8-oxoG content in the dopamine neurons in SN after MPTP treatment, we next assessed the neuroprotective role of MTH1 for the degeneration of dopamine neurons based on a comparison between wild-type and MTH1-null mice. MPTP or saline was administered to wild-type and MTH1-null mice once a day for 5 consecutive days (Figure 6A). The mice were examined for an open field test, rotarod test and the spontaneous basal motor activity in their home cages during the 24 h circadian cycle. There were no significant differences in the motor activity or

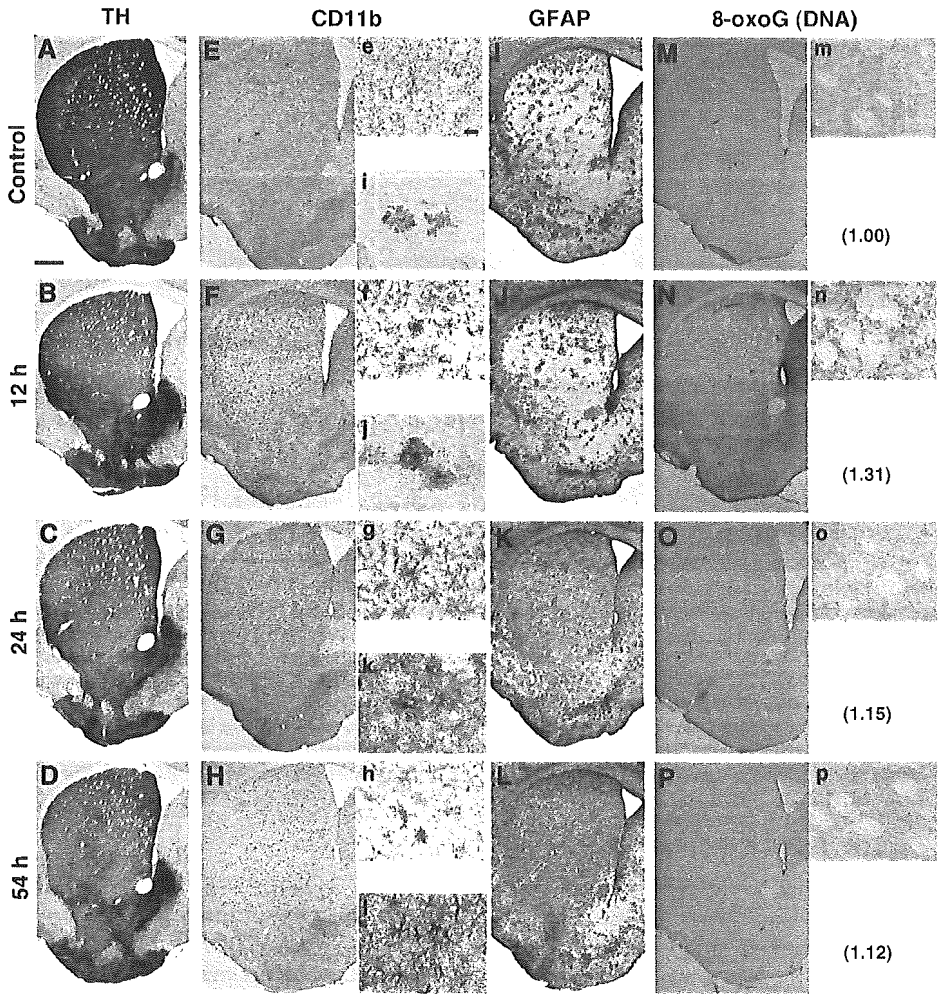

Figure 4 Systemic administration of MPTP transiently increased the accumulation of 8-oxoG in cellular DNA prior to loss of the TH-positive fiber in the striatum. Animals were treated as in Figure 2A. The immunohistochemical detection of TH (**A–D**), CD11b (**E–H**, e–h), GFAP (**I–L**, i–l), and 8-oxoG in DNA (**M–P**, m–p). The control mice (**A**, **E**, e, **I**, i, **M**, m); 12 h after the first MPTP injection (**B**, **F**, f, **J**, j, **N**, n); 24 h after the first injection (**C**, **G**, g, **K**, k, **O**, o); 54 h after the first injection with three injections of MPTP (**D**, **H**, h, **L**, l, **P**, p). The insets in the panels (**e–p**) indicate enlarged view of each section. At 12 h after the MPTP injection, an increased microglial activation was observed in the striatum (**F**, f), and 24 h after the injection, the loss of TH-positive fiber in the striatum, NAc and the OT became apparent (**C**), and an increased astrocytes activation was observed in the striatum (**K**, k), while the 8-oxoG level transiently increased only 12 h after the MPTP injection (**N**, n). Relative densities of 8-oxoG immunoreactivitiy to the control (**M**) are shown in parenthesis. Scale bars (**A–P**), 500 μm; (e–p), 20 μm

motor performance between wild-type and MTH1-null mice before and after MPTP administration (data not shown).

At 7 days after the last MPTP or saline injection, the mice were killed and subjected to immunohistochemistry (Figure 6A). The number of TH-positive neurons in the SNc did not differ between the saline-injected wild-type and MTH1-null mice (Figure 6Ba, b; 6C). A significant reduction in TH immunoreactivitiy was apparent in the SN from both wild-type and MTH1-null mice (Figure 6Bc, d). About 30% reduction in the number of TH-positive neurons across several levels of the SNc was observed in both wild-type and MTH1-null mice after MPTP treatment, and there was no apparent difference between the two groups (Figure 6C). A mild and similar decrease of TH immunoreactivitiy in VTA was also observed in both wild-type and MTH1-null mice after MPTP treatment (Figure 6D).

MTH1-null mice display a more severe reduction of the TH and dopamine transporter (DAT) immunoreactivities in striatal terminal fibers of dopamine neurons after chronic exposure to MPTP

We next examined whether an MTH1 deficiency would augment the reduction of the TH and DAT immunoreactivities in terminal fibers of dopamine neurons in the striatum induced by chronic MPTP administration (Figure 6A). Either TH, DAT or GFAP immunoreactivitiy in the striatum, NAc and OT did not differ between the saline-injected MTH1-null and wild-type mice (Figure 7A, control).

At 7 days after the last MPTP injection, a significant reduction in TH immunoreactivitiy in the striatum, NAc, and OT was observed in wild type and the reduction appeared to

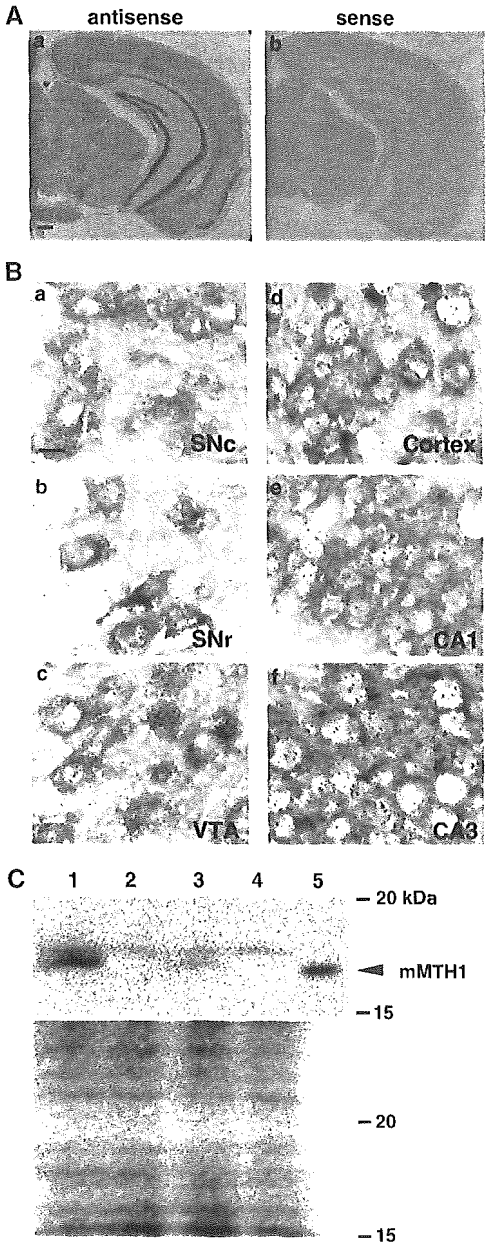

Figure 5 Expression of *Mth1* mRNA in the normal mouse brain. (**A**) The level of *Mth1* mRNA in the coronal midbrain sections prepared from the C57BL/6J male mouse was visualized by *in situ* hybridization with an antisense (a) and sense probe (b). Hybridization signals were detected only with an antisense probe, and they were present in the neurons throughout the brain including the SN and hippocampus. Scale bar, 500 μm. (**B**) Hybridization signals for *Mth1* mRNA were present in the neurons of the SNc (a), SNr (b) and VTA (c) as well as in the neurons scattered throughout the cerebral cortex (d), hippocampal CA1 (e) and CA3 subfields (f). Scale bar: 10 μm. (**C**) The expression level of MTH1 in the striatum was examined by a Western blot analysis using anti-MTH1 (upper). MPTP (30 mg/kg) or saline was administered i.p to wild-type and MTH1-null mice once a day for 5 consecutive days. At 7 days after the last injection, the lysates (100 μg/lane) prepared from isolated striatum and the recombinant mMTH1 (10 pg/lane) were subjected to Western blotting. Lane 1, control wild type; lane 2, control MTH1-null mice; lane 3, MPTP-treated wild type; lane 4, MPTP-treated MTH1-null; lane 5, recombinant mMTH1 (10 pg). The same membrane stained with ponceau was shown (lower)

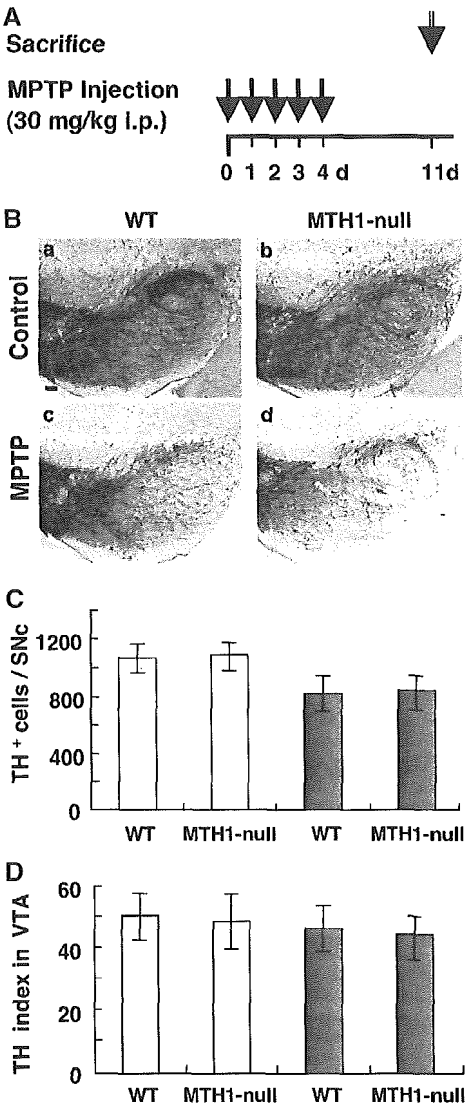

Figure 6 Dopamine neuron loss in the substantia nigra induced by MPTP was not affected by MTH1 deficiency. (**A**) MPTP (30 mg/kg) or saline was administered i.p to wild-type and MTH1-null mice once a day for 5 consecutive days. At 7 days after the last injection, the mice were killed for analyses ($n = 5$ for each group). (**B**) Reduction of TH immunoreactivitiy in the SN 7 days after the last MPTP injection. Sections prepared from wild type (a, c) and MTH1-null mice (b, d), after saline (a, b) or MPTP (c, d) injection were subjected to TH immunohistochemistry. A significant reduction of TH immunoreactivitiy was apparent in the SN from both wild-type and MTH1-null mice after MPTP injection (**c, d**). Scale bar, 100 μm. (**C**) The number of TH-positive neurons in the SNc 7 days after the last MPTP injection decreased by the same degree in both wild-type and MTH1-null mice. The value of the means $\pm$ S.D. for each group ($n = 5$) is shown as a bar graph without (open bars), or with MPTP treatment (gray bars). (**D**) A mild and similar decrease of TH immunoreactivitiy in VTA was observed in both wild-type and MTH1-null mice after MPTP treatment. TH immunoreactivities in the VTA were measured in the sections shown in Figure 6B and the TH indexes are shown as a bar graph with a value of means $\pm$ S.D. for each group ($n = 5$) without (open bars), or with MPTP treatment (gray bars)

be more severe in the MTH1-null mice (Figure 7Ai, m). DAT immunoreactivitiy in the three regions also apparently decreased more in the MTH1-null than in the wild-type mice (Figure 7Aj, n). The immunoreactivities for TH and DAT were

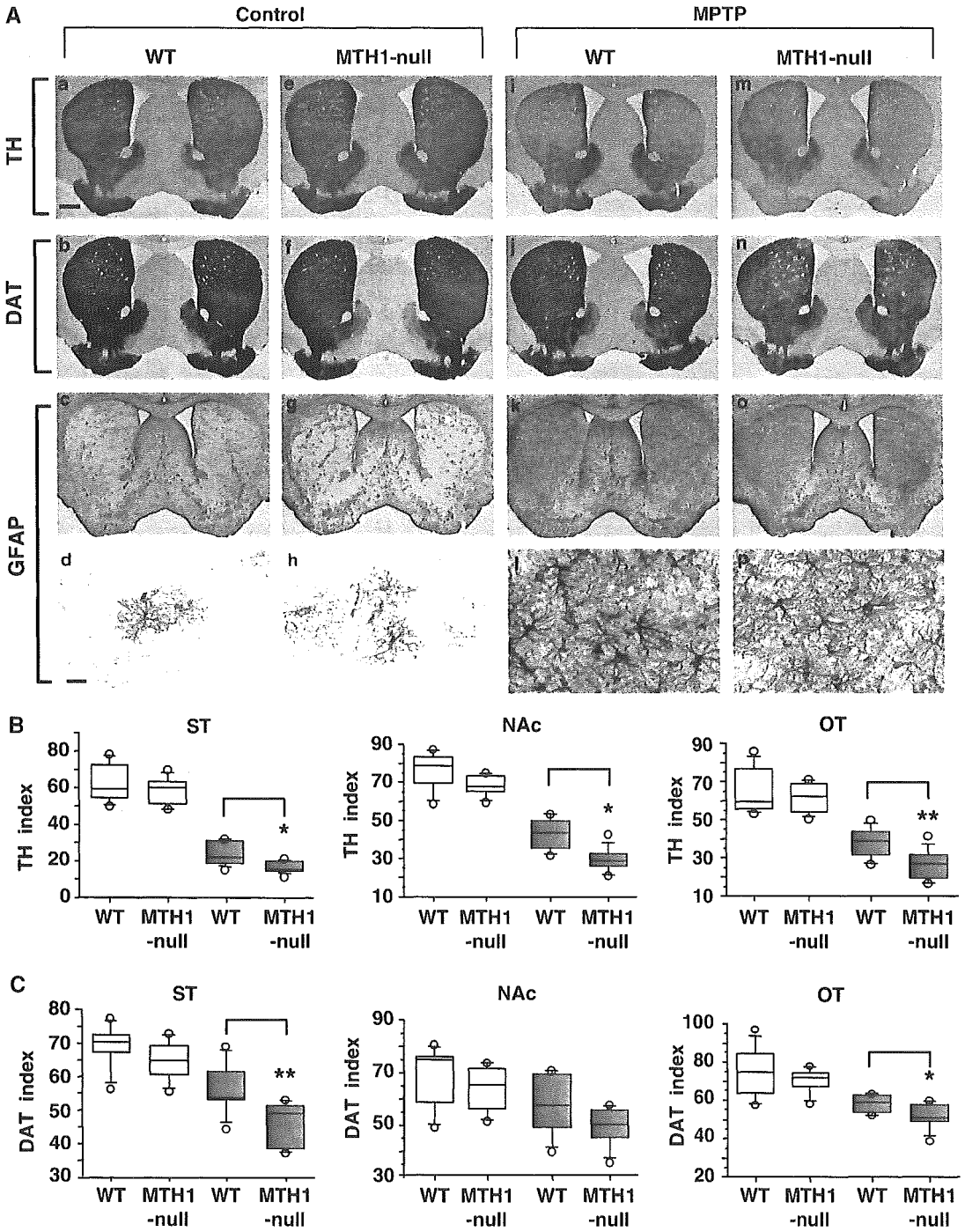

Figure 7 MTH1-null mice display an increased reduction of TH and DAT immunoreactivities in striatal terminal fibers of dopamine neurons after chronic exposure to MPTP. (**A**) Striatal immunoreactivities for TH, DAT, and GFAP were examined in the sections prepared from the mice administered with saline (Control, a–h) or MPTP (MPTP, i–p), as described in Figure 6A. Wild type (a–d, i–l); MTH1-null mice (e–h, m–p). The magnification of images (c, g, k, o) are shown (d, h, l, p), respectively. Scale bars (a–c, e–g, i–k, m–o) 500 μm; (d, h, l, p) 20 μm. (**B**) TH immunoreactivities in the striatum, NAc and OT were measured in the sections shown in Figure 7A, and TH indexes are shown in a box and whisker plot ($n=5$). In each plot, the boxes are drawn with the ends at the quartiles, and the statistical median is shown as a horizontal line in the box. The whiskers extended to the farthest points which are not outliers (circles). TH indexes in striatum, NAc, and OT of MTH1-null mice were significantly lower than those of wild type (WT) after MPTP injection (Mann–Whitney *U*-test, $^{**}P<0.01$, $^{*}P<0.02$). Control, open boxes; MPTP treated, gray boxes. (**C**) DAT immunoreactivities in the striatum, NAc and OT were measured in the sections shown in Figure 7A, and DAT indexes are shown in a box-and-whisker-plot ($n=4\sim5$), as in B. DAT indexes in striatum and OT of MTH1-null mice were also significantly lower than those of wild type after MPTP injection (Mann–Whitney *U*-test, $^{**}P<0.01$, $^{*}P<0.05$)

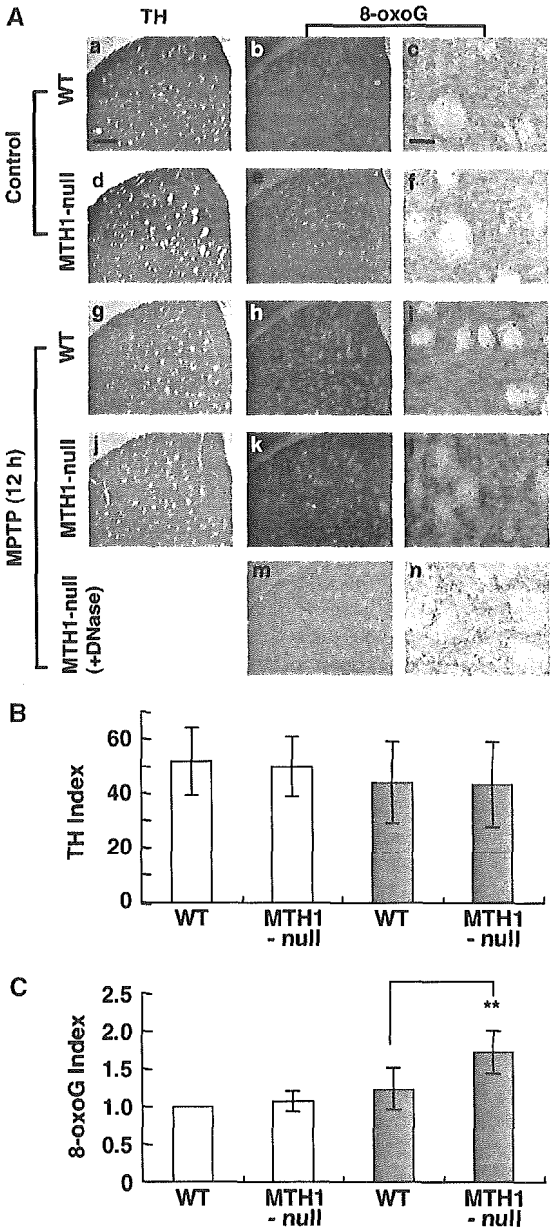

Figure 8 Increased accumulation of 8-oxoG in the striatum of MTH1-null mice after MPTP administration. (**A**) Striatal immunoreactivities for TH (a, d, g, j) and 8-oxoG in DNA (b, c, e, f, h, i, k, l) were examined in the sections prepared 12 h after the administration of saline (control) or MPTP. To detect 8-oxoG in DNA, the sections were pretreated only with RNase and reacted with the N45.1 mAb. A section was further pretreated with DNase, and then was subjected to the immunohistochemistry using the same antibody (m, n). Wild type (a–c, g-i); MTH1-null mice (d–f, j–n). The magnification of images (b, e, h, k, m) are shown (c, f, i, l, n), respectively. Scale bars (a, b, d, e, g, h, j, k, m) 300 μm; (c, f, i, l, n) 40 μm. (**B**) Immunoreactivities for TH in the sections shown in Figure 8A were digitized, and TH index in each sample was determined ($n=4$ per group). The TH index is shown as a bar graph with the means $\pm$S.D. Open bar: control; gray bar, MPTP treated. (**C**) Immunoreactivities for 8-oxoG in the sections shown in Figure 8A were digitized, and 8-oxoG index in each sample was determined ($n=4$ per group). The relative value of each 8-oxoG index to that of control is shown as a bar graph with the means $\pm$S.D. Open bar: control; gray bar, MPTP treated. The 8-oxoG index was increased more significantly in MTH1-null mice in comparison to wild type (Mann–Whitney *U*-test, $^{**}P<0.01$)

digitized and their indexes were compared between the wild-type and MTH1-null mice. TH indexes in striatum, NAc, and OT of MPTP-treated MTH1-null mice were significantly lower than those of the MPTP-treated wild type (Figure 7B). The DAT indexes also decreased significantly more in MPTP-treated MTH1-null mice than in MPTP-treated wild type, especially in the striatum and OT, and to a lesser extent in NAc (Figure 7C).

GFAP immunoreactivitiy in the striatum similarly increased in both the MPTP-treated wild-type and MTH1-null mice, in comparison to the control (Figure 7A, GFAP). There was no significant difference of the GFAP immunoreactivitiy between the MPTP-treated wild-type and MTH1-null mice (data not shown).

These findings indicated that an MTH1 deficiency augments the MPTP-provoked reduction of TH and DAT immunoreactivities in the terminal fibers of dopamine neurons or their dysfunction in the striatum, NAc or OT.

MTH1 deficiency augments the MPTP-induced accumulation of 8-oxoG in the striatum

To compare the extent of 8-oxoG in cellular DNA in the striatum after MPTP injection in wild-type and MTH1-null mice, the mice were injected with MPTP (30 mg/kg) and then were killed 12 h after the injection. At 12 h after MPTP injection, terminal loss of dopamine neurons was apparent in the striatum of MTH1-null mice at the same degree as that seen in wild type (Figure 8A, TH). In the same sections, an increase of 8-oxoG immunoreactivitiy in the cellular DNA was observed in the striatum of wild type (Figure 8Ah, i), and the increase was apparently higher in the MTH1-null mice (Figure 8Ak, l). These immunoreactivities largely decreased after the pretreatment of the sections with DNase (Figure 8Am, n), thus indicating that 8-oxoG in the striatum are mostly in the cytoplasmic DNA, namely, mitochondrial DNA. Immunoreactivities for TH and 8-oxoG in the striatum were digitized, and the level of TH and 8-oxoG in each sample was determined. The TH indexes in striatum of MPTP-treated MTH1-null mice were almost the same level as those of the MPTP-treated wild type (Figure 8B). However, the 8-oxoG indexes in the striatum of the MPTP-treated MTH1-null mice were significantly higher than those of the MPTP-treated wild type (Figure 8C).

Furthermore, we confirmed that the terminal fibers of dopamine neurons in striatum were indeed rich in mitochondria, based on a laser scanning confocal microscopy analysis of TH and cytochrome *C* in the striatum of wild-type mouse (Figure 9A). Most TH signals in the striatum were largely merged with signals for cytochrome *C*, and spiny neurons in the striatum, which are TH negative, also exhibited intense cytochrom *C* signals surrounding their nuclei, thus confirming that both TH-positive terminal fibers of dopamine neurons and the postsynaptic spiny neurons are rich in mitochondria. At 12 h after MPTP injection, strong 8-oxoG immunoreactivities were detected in the striatum of MTH1-null mice but not wild type (Figure 9Ba, f). The 8-oxoG signals exhibited a fiber-like shape and were distributed along with TH-positive fibers, and most of them were colocalized in MTH1-null mice (Figure 9j). It is noteworthy that there was not much 8-oxoG

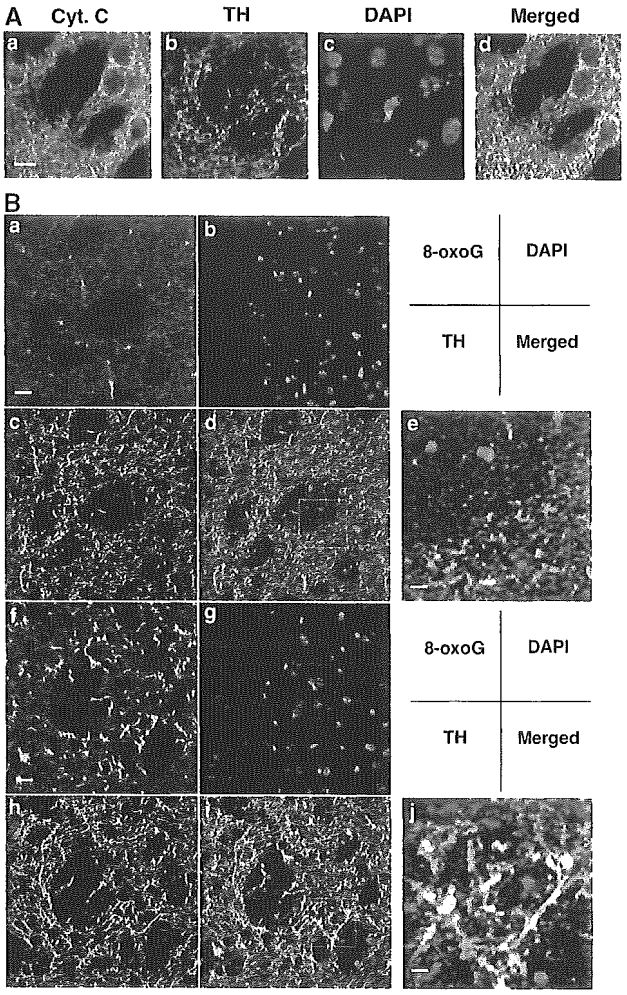

Figure 9 Increased accumulation of 8-oxoG in mitochondrial DNA in the striatal nerve terminals of dopamine neurons in MTH1-null mice after MPTP administration. (**A**) The localization of cytochrome *C* in the striatal terminal fibers of dopamine neurons determined by laser scanning confocal microscopy. The sections from wild-type mouse were stained for cytochrome *C* (Cyt. *c*) (a), TH (b), nuclear DNA with DAPI (c), and the merged image was shown (d). Scale bar: 10 μm. (**B**) The localization of 8-oxoG in the striatal terminal fibers of dopamine neurons determined by laser scanning confocal microscopy. The sections prepared from wild-type (a–e) and MTH1-null mice (f–j) 12 h after MPTP injection (30 mg/kg, i.p.) were stained for 8-oxoG in DNA with the N45.1 mAb (a, f), nuclear DNA with DAPI (b, g), TH (c, h), and their merged images were shown (d, i). The sections were pretreated only with RNase. Scale bar: 20 μm. Each part of images shown in dotted box (d, i) was magnified (e, j). Scale bar: 5 μm

immunoreactivitiy in the cytoplasm of spiny neurons. We thus concluded that 8-oxoG accumulated mostly in the mitochondrial DNA in the striatal nerve terminals of dopamine neurons in the MTH1-null mice 12 h after MPTP injection.

The HPLC–MS/MS analysis revealed that the contents of 8-oxoG in nuclear DNA prepared from three regions of the brains, especially other brain region that contains striatum, thalamus and brainstem, slightly increased 7 days after the last injection of MPTP, both in wild-type and MTH1-null mice (Table 1). The amounts of 8-oxoG did not increase in the liver from MPTP-treated wild-type and MTH1-null mice.

Discussion

In the present study, we, for the first time, revealed that the accumulation of oxidized base, 8-oxoG in DNA and RNA in the nigrostriatal dopamine neurons significantly increases during neuronal dysfunction in the mouse brain induced by the systemic administration of MPTP, and furthermore demonstrated that the accumulation of 8-oxoG in the mitochondrial DNA in the terminal fibers of dopamine neurons is one of causes for the neuronal dysfunction of dopamine neurons, which can be minimized by the sanitization of the nucleotide pool by MTH1 with its oxidized purine nucleoside triphosphatase.

MPTP systemically administered is converted to 1-methyl-4-phenylpryridinium (MPP^+), mostly in glial cells, and then MPP^+ can be specifically taken up by dopamine neurons through DAT. MPP^+ which accumulates in dopamine neurons binds to complex I of the respiratory chain in mitochondria and blocks the electron transport, thus leading to an energy failure with ATP depletion as well as an increase of electron leakage from the respiratory chain resulting in the formation of free radicals.[15,16] In addition, dopamine neurons are likely to be exposed to increased levels of oxidative stress caused by the metabolic products of dopamine itself in comparison to the other parts of brain. MPP^+ also induces a massive release of vesicular dopamine to the cytosol[17] or an increased dopamine turnover, and it is thus expected that oxidative stress in the dopamine neurons is significantly and specifically increased in such MPTP-administered animals.[18,19] Furthermore, the oxidation of dopamine stoichiometrically produces hydrogen peroxide which reacts with Fe^{2+} ion to form hydroxyradical by the Fenton reaction. Hydroxyradical is the most reactive free radicals and it easily oxidizes almost all biomolecules, such as lipids, proteins and nucleic acids, thus resulting in cellular dysfunction or cell death.[20,21] Since the mitochondrial dysfunction and oxidative stress induced by MPTP are remarkably similar to that seen in the PD brain,[22,23] studies in genetics and biochemical pathways involved in MPTP toxicity have provided clues to a better understanding of idiopathic PD.

An increased lipid peroxidation and chemical modification of proteins are common features in MPTP-induced PD model, and there has been only one literature reporting that MPTP induces the accumulation of 8-oxoG, an oxidized form of guanine, in the model.[24] Our present study clearly demonstrated that the accumulation of 8-oxoG in the cellular RNA and DNA significantly increased in SN 12–24 h after a single administration of MPTP, confirming the previous observation,[24] moreover, we showed that the accumulation of 8-oxoG was more remarkable in striatum than in SN. Especially, 8-oxoG accumulated in the mitochondrial DNA in the striatal nerve terminals of dopamine neurons earlier than the decrease of TH immunoreactivitiy in the striatum, or earlier than accumulation of 8-oxoG in cellular RNA or DNA in the SN, where a loss of TH-positive dopamine neurons becomes apparent after the repeated administration of MPTP. These observations strongly suggest that MPP^+ triggers a degeneration of the dopamine neurons from their terminals in the striatum, in a retrograde manner, as reported previously.[25] We further observed that microglias and astrocytes were

significantly activated in striatum or SN 12–24 h after a single administration of MPTP. It has been shown that the activated microglias or astrocytes produce more extracellular superoxide by NADPH oxidase, thus further increasing the oxidative stress in the striatum or SN.[26,27] In the present study, however, we found that dopamine neuron loss in SNc induced by MPTP was not affected by MTH1 deficiency, that is, only 20% of dopamine neurons in SNc were lost 7days after the last MPTP injection both wild-type and MTH1-null mice (Figure 6). Thus, it is likely that the dose of MPTP was not enough to reveal an increased vulnerability of MTH1-null dopamine neurons in the SNc, or it may take much longer time to exhibit their increased vulnerability.

We previously demonstrated that the accumulation of 8-oxoG in the mitochondrial DNA of MTH1-null cells induced by hydrogen peroxide treatment results in mitochondrial dysfunction and finally in pyknotic cell death which is independent of general caspases or polyADP-ribose polymerase, but such cell death is very efficiently suppressed by an overexpression of human MTH1.[14] Since MTH1 possesses an oxidized purine nucleoside triphosphatase activity which efficiently hydrolyzes 2-OH-dATP, 8-oxo-dGTP, 8-oxo-dATP and 2-OH-ATP or 8-oxo-ATP, to a lesser extent 8-oxo-GTP, the disruption of the *Mth1* gene must result in the accumulation of these oxidized purine nucleoside triphosphates in the dopamine neurons after MPTP administration. In the present study, we observed that the accumulation of 8-oxoG in the mitochondrial DNA of the terminals of dopamine neurons significantly increased in MTH1-null in comparison to wild-type mice, thus suggesting that various oxidized purine nucleoside triphosphates as well as 8-oxo-dGTP accumulate in the terminals of dopamine neurons and their incorporation into mitochondrial DNA is increased in MTH1-null mice. Furthermore, we showed that an MTH1 deficiency augments the MPTP-provoked reduction of TH and DAT immunoreactivities in the terminal fibers of dopamine neurons in the striatum. These results together strongly suggest that increased levels of various oxidized purine nucleoside triphosphates, including 8-oxo-dGTP, induce a dysfunction of the terminal fibers of dopamine neurons.

Using mutant human MTH1 which hydrolyzes 8-oxo-dGTP but not 2-OH-dATP, or vice versa, we showed that the accumulation of 8-oxo-dGTP and 2-OH-dATP, at least, in the cells results in mitochondrial dysfunction accompanied with electron-dense deposits in the mitochondria, and cell death in murine fibroblasts,[14] however, it is still unclear as to how the oxidized purine nucleoside triphosphates accumulated or those incorporated into mitochondrial DNA causes such mitochondrial dysfunction and cell death. It has been shown that oxidative damage to mitochondrial DNA increases with age in the human brain, especially in the SN, and it can induce G:C to T:A and A:T to C:G transversion mutations,[28] which are known to be caused by 8-oxoG or 2-OH-A,[1] thus suggesting that such mutations in mitochondrial DNA might cause mitochondrial dysfunction. It has been shown that electron-dense deposits in the mitochondria are formed in the MPTP-induced PD model,[29] thus indicating that the induction of mitochondrial dysfunction is one of the major pathways that cause the degeneration of dopamine neurons. We are now trying to identify the signal transduction pathway that triggers cell death following an accumulation of 8-oxo-dGTP or 2-OH-dATP in the MTH1-null cells.

In PD patient brains, we found a markedly increased expression of MTH1 accompanied with a significant accumulation of 8-oxoG in the cytoplasm of surviving dopamine neurons in the SN.[9] Furthermore, we recently also found a highly increased expression of a mitochondrial form of OGG1 (hOGG1–2a) in dopamine neurons in the SN of PD patient brain, thus supporting our hypothesis that 8-oxoG accumulated in mitochondrial DNA is somehow toxic to dopamine neurons.[30] The present study strongly suggests that the increased expression of MTH1 in the dopamine neurons of PD patients may attenuate their progressive degeneration, and an experimental demonstration of this hypothesis would shed light on the development of new strategies for the therapeutic treatment of PD.

Materials and Methods

Antibodies

Mouse N45.1 mAb (1 : 100), which preferentially recognizes 8-oxoG in DNA, was obtained from JaICA (Fukuroi, Japan), while mouse 15A3 mAb (1 : 1200), which recognizes 8-oxoG in both DNA and RNA was obtained from QED Bioscience. To prepare the antibodies preadsorbed by antigen, the N45.1 or 15A3 mAb was mixed with 8-oxo-dG (Sigma) or dG (Yamasa, Japan) at a molar ratio of 1 : 100, and were incubated for 12 h at 4°C. Rabbit anti-GFAP polyclonal antibodies (1 : 15000) were purchased from Dako. Rabbit anti-TH polyclonal antibodies (1 : 2000), and rat anti-DAT mAb (1 : 8000) (DAT-Nt, MAB369) were obtained from Chemicon. Rat mAb, MAC-1 (1 : 100) against mouse CD11b was obtained from Serotec. Rabbit anti-VDAC polyclonal antibodies were described previously.[31] Mouse anticytochrome *C* mAb (1 : 500) was purchased from BD Biosciences. Alexa Fluor-labeled second antibodies were obtained from Invitrogen.

Animals

We previously established *Mth1* gene-knockout mice.[13] Heterozygous mice (*Mth1*$^{+/-}$) backcrossed to C57BL/6J (Clea Japan Inc., Tokyo, Japan) for more than 12 generations were maintained, thereby ensuring a standard C57BL/6J genetic background.[32] In the present study, the C57BL/6J strain was considered to be a wild-type mouse. MTH1-null (*Mth1*$^{-/-}$) mice obtained by the mating of the heterozygous *Mth1*$^{+/-}$ mice were bred only one generation to yield MTH1-null offsprings for the experiments. Animals were maintained in an air-conditioned, light time-controlled, specific-pathogen-free room. The handling and killing of all animals were carried out in accordance with the national prescribed guidelines, and ethical approval for the studies was granted by the Animal Experiment Committee of Kyushu University.

Experimental design and MPTP treatment

Male mice (10–12 weeks old) were used for this study. Mice were injected i.p. once a day for 5 consecutive days, with either saline (vehicle) or MPTP-HCl (30 mg/kg free base, Sigma) dissolved in saline. To analyze the acute phase response after MPTP administration, mice were killed at various time points, ranging 0, 6, 12, 24 h after the first injection on the day 0, and 6 h after the third injection on the day 2. To analyze the chronic effects of MPTP, mice were killed 7 days after the fifth injection on the

day 4. Each experimental design is shown in Figure 2A and Figure 6A, respectively.

Tissue processing

Animals deeply anesthetized with pentobarbital (30 mg/kg i.p.), were perfused intracardially with saline followed by cold 4% paraformaldehyde (PFA) in 0.1 M PBS. The brains were removed, immersed for 12 h in the same 4% PFA fixative at 4°C, and cryoprotected in 20%, 30% sucrose in PBS for 48 h at 4°C. The brains were then frozen and stored at −80°C until use. Serial coronal sections (40 μm thickness) were cut on a cryostat, collected as free-floating sections in PBS or PBS-T (Triton X, 0.3%), and processed immediately for immunohistochemistry. Coronal sections (10 μm thickness) were cut on a cryostat, and then were mounted on slides and stored at −80°C until they were used for *in situ* hybridization.

Pretreatment of free-floating section for detection of 8-oxoG

To detect 8-oxoG in RNA, free-floating sections were directly subjected to immunohistochemistry with the 15A3 mAb, without any pretreatment. To eliminate cellular RNA, the sections were incubated in 10 mM Tris-HCl (pH7.5), 15 mM NaCl containing DNase-free RNase (5 mg/ml of heat-inactivated RNase A, Sigma) for 60 min at 37°C, prior to incubation with a proper primary antibody. To detect 8-oxoG in cellular DNA other than nuclear DNA, the RNase-treated sections were directly subjected to immunohistochemistry with the N45.1 mAb. To detect 8-oxoG in nuclear DNA, the RNase-treated sections were further treated with 3 N HCl at room temperature for 30 min, thus denaturing the nuclear DNA, and then sections were subjected to immunohistochemistry with the N45.1 mAb. To eliminate cellular DNA, the sections were incubated in 50 mM Tris-HCl (pH7.5), 0.1 mM $MgCl_2$ containing RNase-free DNase I (1000 U/ml, Sigma) for 60 min at 37°C, following incubation with DNase-free RNase.

Immunohistochemistry

Free-floating sections with an appropriate pretreatment were incubated in Block Ace, (Dainippon Pharmaceutical, Japan) for 30 min at room temperature, and then were incubated with each appropriately diluted primary antibody in 10% Block Ace, at 4°C overnight. The rinsed sections were immersed in a solution of 3% H_2O_2 in methanol/PBS (1 : 1) for 5 min at root temperature, and then were processed by Vectastain ABC kit (Vector Labo.) with a proper biotinylated secondary antibody, and the peroxidase reaction product was detected using 3′3′-diaminobenzidine-tetrahydrochloride (DAB, Vector). All sections were then washed in PBS, mounted on slides, and coverslipped. Digital images were acquired using Axioskop2 plus equipped with a CCD camera, AxioCam (Carl Zeiss), or using LeicaZoom2000 (Leica Mycrosystems) equipped with a digital camera, Cyber-shot (Sony, Japan). In order to ensure the quantitative measurement of each immunoreactivitiy, all sections from each experimental animal and group to be compared were processed in parallel by immunohistochemistry.

Laser scanning confocal microscopy

Free-floating sections incubated with a proper primary antibody were further incubated with a proper Alexa Fluor-labeled second antibody for 45 min at room temperature. The sections were incubated in a solution containing DAPI (0.05 μg/ml, Sigma) for 10 min at room temperature, and mounted on slides with Vectashield (Vector). Confocal images were acquired under Eclipse TE300 (Nikon, Japan) equipped with the Radiance 2100 laser scanning confocal microscope system (Bio-Rad Labo.), or under LSM 510 META (Carl Zeiss). All sections from each experimental animal and group to be compared were processed in parallel.

Quantitative morphometric analysis

All acquired digital images were processed uniformly at a threshold in a gray scale mode to subtract any background corresponding to the area without tissue by Adobe Photoshop version 5.5 (Adobe Systems). The OD of each immunoreactivitiy in a given area for 8-oxoG, TH, DAT, GFAP, respectively, was measured using the Image Gauge version 3.2 (FUJIFILM, Japan). From each individual animal, four representative sections were measured and the mean OD was calculated as an immunoreactivitiy index for each animal. The number of dopamine neurons in the SNc was estimated by counting all TH-positive neurons of two hemispheres from five coronal sections (40 μm thick) per animal that were distributed every 120 μm along the rostral–caudate axis of the SN (−3.08 to −3.64 mm caudal to bregma).[33] In order to quantitate 8-oxoG immunoreactivitiy in TH-positive neurons in SNc, fluorescent signals for 8-oxoG in nuclear DNA of the TH-positive neurons were selectively extracted from the confocal images for TH and 8-oxoG immunofluorescence, using the Adobe Photoshop. The OD of fluorescent signals for 8-oxoG were measured by using Image Gauge. In all, 15–30 TH-positive neurons in five sections from each animal were analyzed, and the mean OD was calculated as 8-oxoG index per a TH-positive neuron for each animal. All quantitative analyses were performed by an individual unaware of the experimental treatments.

In situ hybridization of mouse *Mth1* mRNA

A digoxigenin-labeled single-stranded RNA probe was prepared using the Digoxigenin RNA Labeling Kit (Roche), according to the manufacturer's instructions. pGEM-3Zf plasmid (Promega) carrying mouse *Mth1* cDNA was transcribed with SP6 or T7 RNA polymerase in the presence of digoxigenin-labeled UTP (Roche) to obtain the sense and antisense riboprobes. *In situ* hybridization was performed using the Ventana Discovery instrument (Ventana Medical Systems) according to the manufacturer's instructions. The sections were incubated with alkaline phosphatase-conjugated antidigoxigenin antibody (1 : 500, Roche). Alkaline phosphatase reaction product was detected using 5-bromo-4-chloro-3-indolyl phosphate/nitro blue tetrazolium (Sigma).

Western blotting

The brain samples were homogenized at 4°C in five volumes of lysis buffer containing 50 mM Tris-HCl pH 8.0, 150 mM NaCl, 0.5% sodium deoxycholate, 1% NP40, 0.1% SDS, and protease inhibitor cocktail (Nacalai Tesque, Japan), followed by sonication. The brain lysates were subjected to SDS-PAGE (15%) followed by Western blotting using anti-MTH1 (3.0 μg/ml),[34] according to a previously described method.[35] After blotting, the membrane was incubated with 0.5% ponceau S (MP Biomedical, Germany) to quantitate the amount of protein on the membrane. Recombinant mouse MTH1 (mMTH1) expressed in *E. coli* BL21 cells carrying pET3a : mMTH1 was used as a standard.

HPLC–MS/MS analysis

The nuclear DNA was prepared from the tissue specimens and were subjected to an HPLC–MS/MS analysis of 8-oxoG, according to a

previously described method.[36] Brain was separated to three regions, cerebrum, cerebellum and other brain region that contains striatum, thalamus and brainstem, prior to DNA extraction.

Acknowledgements

We thank Drs. Yasuhide Mitsumoto, Masami Nakai, Daisuke Tsuchimoto for their helpful discussions, Setsuko Kitamura, Naomi Adachi, Akemi Matsuyama and Keiko Aiura for their technical assistance, Dr. Jun-ichi Kira for providing us with the opportunity to conduct this study, Dr. B Quinn for comments on the manuscript. This work was supported by grants from CREST, Japan Science and Technology Agency, the Ministry of Education, Culture, Sports, Science, and Technology of Japan (Grant number: 16012248), and the Japan Society for the Promotion of Science (Grant numbers: 15590347, 16390119).

References

1. Nakabeppu Y, Tsuchimoto D, Furuichi M and Sakumi K (2004) The defense mechanisms in mammalian cells against oxidative damage in nucleic acids and their involvement in the suppression of mutagenesis and cell death. Free Radic. Res. 38: 423–429
2. Sekiguchi M and Tsuzuki T (2002) Oxidative nucleotide damage: consequences and prevention. Oncogene 21: 8895–8904
3. Nakabeppu Y (2001) Molecular genetics and structural biology of human MutT homolog, MTH1. Mutat. Res. 477: 59–70
4. Nakabeppu Y, Tsuchimoto D, Ichinoe A, Ohno M, Ide Y, Hirano S, Yoshimura D, Tominaga Y, Furuichi M and Sakumi K (2004) Biological significance of the defense mechanisms against oxidative damage in nucleic acids caused by reactive oxygen species: from mitochondria to nuclei. Ann. NY Acad. Sci. 1011: 101–112
5. Shigenaga MK, Hagen TM and Ames BN (1994) Oxidative damage and mitochondrial decay in aging. Proc. Natl. Acad. Sci. USA 91: 10771–10778
6. Kasai H and Nishimura S (1984) Hydroxylation of deoxyguanosine at the C-8 position by ascorbic acid and other reducing agents. Nuc. Acids Res. 12: 2137–2145
7. Iida T, Furuta A, Kawashima M, Nishida J, Nakabeppu Y and Iwaki T (2001) Accumulation of 8-oxo-2′-deoxyguanosine and increased expression of hMTH1 protein in brain tumors. Neuro-oncol 3: 73–81
8. Zhang J, Perry G, Smith MA, Robertson D, Olson SJ, Graham DG and Montine TJ (1999) Parkinson's disease is associated with oxidative damage to cytoplasmic DNA and RNA in substantia nigra neurons. Am. J. Pathol. 154: 1423–1429
9. Shimura-Miura H, Hattori N, Kang D, Miyako K, Nakabeppu Y and Mizuno Y (1999) Increased 8-oxo-dGTPase in the mitochondria of substantia nigral neurons in Parkinson's disease. Ann. Neurol. 46: 920–924
10. Nunomura A, Perry G, Aliev G, Hirai K, Takeda A, Balraj EK, Jones PK, Ghanbari H, Wataya T, Shimohama S, Chiba S, Atwood CS, Petersen RB and Smith MA (2001) Oxidative damage is the earliest event in Alzheimer disease. J. Neuropathol. Exp. Neurol. 60: 759–767
11. Kikuchi H, Furuta A, Nishioka K, Suzuki SO, Nakabeppu Y and Iwaki T (2002) Impairment of mitochondrial DNA repair enzymes against accumulation of 8-oxo-guanine in the spinal motor neurons of amyotrophic lateral sclerosis. Acta. Neuropathol. 103: 408–414
12. Furuta A, Iida T, Nakabeppu Y and Iwaki T (2001) Expression of hMTH1 in the hippocampi of control and Alzheimer's disease. Neuroreport 12: 2895–2899
13. Tsuzuki T, Egashira A, Igarashi H, Iwakuma T, Nakatsuru Y, Tominaga Y, Kawate H, Nakao K, Nakamura K, Ide F, Kura S, Nakabeppu Y, Katsuki M, Ishikawa T and Sekiguchi M (2001) Spontaneous tumorigenesis in mice defective in the MTH1 gene encoding 8-oxo-dGTPase. Proc. Natl. Acad. Sci. USA 98: 11456–11461
14. Yoshimura D, Sakumi K, Ohno M, Sakai Y, Furuichi M, Iwai S and Nakabeppu Y (2003) An oxidized purine nucleoside triphosphatase, MTH1, suppresses cell death caused by oxidative stress. J. Biol. Chem. 278: 37965–37973
15. Nicklas WJ, Vyas I and Heikkila RE (1985) Inhibition of NADH-linked oxidation in brain mitochondria by 1-methyl-4-phenyl-pyridine, a metabolite of the neurotoxin, 1-methyl-4-phenyl-1,2,5,6-tetrahydropyridine. Life Sci. 36: 2503–2508
16. Ramsay RR, Krueger MJ, Youngster SK, Gluck MR, Casida JE and Singer TP (1991) Interaction of 1-methyl-4-phenylpyridinium ion (MPP+) and its analogs with the rotenone/piericidin binding site of NADH dehydrogenase. J. Neurochem. 56: 1184–1190
17. Lotharius J and O'Malley KL (2000) The parkinsonism-inducing drug 1-methyl-4-phenylpyridinium triggers intracellular dopamine oxidation. A novel mechanism of toxicity. J. Biol. Chem. 275: 38581–38588
18. Schmidt N and Ferger B (2001) Neurochemical findings in the MPTP model of Parkinson's disease. J. Neural Transm. 108: 1263–1282
19. Przedborski S and Vila M (2003) The 1-methyl-4-phenyl-1,2,3,6-tetrahydropyridine mouse model: a tool to explore the pathogenesis of Parkinson's disease. Ann. NY Acad. Sci. 991: 189–198
20. Karam LR, Bergtold DS and Simic MG (1991) Biomarkers of OH radical damage *in vivo*. Free Radic. Res. Commun. 12–13 (Part 1): 11–16
21. Halliwell B (1992) Reactive oxygen species and the central nervous system. J. Neurochem. 59: 1609–1623
22. Schapira AH (1997) Mitochondrial dysfunction and oxidative damage in Parkinon's disease In *Mitochondria and Free Radicals in Neurodegenarative Diseases* Beal M, Howell N and Bódis-Wollner I (eds) (New York: Wiley-Liss Inc.) pp. 343–359
23. Mizuno Y, Yoshino H, Ikebe S, Hattori N, Kobayashi T, Shimoda-Matsubayashi S, Matsumine H and Kondo T (1998) Mitochondrial dysfunction in Parkinson's disease. Ann. Neurol. 44: S99–S109
24. Chen L-J, Gao Y-Q, Li X-J, Shen D-H and Sun F-Y (2005) Melatonin protects against MPTP/MPP+-induced mitochondrial DNA oxidative damage *in vivo* and *invitro*. J. Pineal Res. 39: 34–42
25. Nakai M, Mori A, Watanabe A and Mitsumoto Y (2003) 1-methyl-4-phenylpyridinium (MPP^+) decreases mitochondrial oxidation-reduction (REDOX) activity and membrane potential ($\Delta\psi_m$) in rat striatum. Exp. Neurol. 179: 103–110
26. Czlonkowska A, Kohutnicka M, Kurkowska-Jastrzebska I and Czlonkowski A (1996) Microglial reaction in MPTP (1-methyl-4-phenyl-1,2,3,6-tetrahydropyridine) induced Parkinson's disease mice model. Neurodegeneration 5: 137–143
27. Kurkowska-Jastrzebska I, Wronska A, Kohutnicka M, Czlonkowski A and Czlonkowska A (1999) The inflammatory reaction following 1-methyl-4-phenyl-1,2,3, 6-tetrahydropyridine intoxication in mouse. Exp. Neurol. 156: 50–61
28. Simon DK, Lin MT, Zheng L, Liu GJ, Ahn CH, Kim LM, Mauck WM, Twu F, Beal MF and Johns DR (2004) Somatic mitochondrial DNA mutations in cortex and substantia nigra in aging and Parkinson's disease. Neurobiol. Aging 25: 71–81
29. Song DD, Shults CW, Sisk A, Rockenstein E and Masliah E (2004) Enhanced substantia nigra mitochondrial pathology in human alpha-synuclein transgenic mice after treatment with MPTP. Exp. Neurol. 186: 158–172
30. Fukae J, Takanashi M, Kubo S-i, Nishioka K-i, Nakabeppu Y, Mori H, Mizuno Y and Hattori N (2005) Expression of 8-oxoguanine DNA glycosylase (OGG1) in Parkinson's disease and related neurodegenerative disorders. Acta Neurophathol. 109: 256–262
31. Alam TI, Kanki T, Muta T, Ukaji K, Abe Y, Nakayama H, Takio K, Hamasaki N and Kang D (2003) Human mitochondrial DNA is packaged with TFAM. Nuc. Acids Res. 31: 1640–1645
32. Sakumi K, Tominaga Y, Furuichi M, Xu P, Tsuzuki T, Sekiguchi M and Nakabeppu Y (2003) *Ogg1* knockout-associated lung tumorigenesis and its suppression by *Mth1* gene disruption. Cancer Res. 63: 902–905
33. Franklin KB and Paxinos G (2001) *The Mouse Brain in Stereotaxic Coordinates* (New York: Academic Press)
34. Kakuma T, Nishida J, Tsuzuki T and Sekiguchi M (1995) Mouse MTH1 protein with 8-oxo-7,8-dihydro-2′-deoxyguanosine 5′-triphosphatase activity that prevents transversion mutation. cDNA cloning and tissue distribution. J. Biol. Chem. 270: 25942–25948
35. Tsuchimoto D, Sakai Y, Sakumi K, Nishioka K, Sasaki M, Fujiwara T and Nakabeppu Y (2001) Human APE2 protein is mostly localized in the nuclei and to some extent in the mitochondria, while nuclear APE2 is partly associated with proliferating cell nuclear antigen. Nuc. Acids Res. 29: 2349–2360
36. Tsuruya K, Furuichi M, Tominaga Y, Shinozaki M, Tokumoto M, Yoshimitsu T, Fukuda K, Kanai H, Hirakata H, Iida M and Nakabeppu Y (2003) Accumulation of 8-oxoguanine in the cellular DNA and the alteration of the OGG1 expression during ischemia-reperfusion injury in the rat kidney. DNA Repair 2: 211–229

The EMBO Journal (2005) 24, 2590–2601 | © 2005 European Molecular Biology Organization | All Rights Reserved 0261-4189/05
www.embojournal.org

THE EMBO JOURNAL

Stress response gene *ATF3* is a target of c-*myc* in serum-induced cell proliferation

Kiyoshi Tamura[1,2], Bayin Hua[1], Susumu Adachi[3], Isil Guney[4], Junya Kawauchi[1], Masaki Morioka[1], Mimi Tamamori-Adachi[1], Yujiro Tanaka[1], Yusaku Nakabeppu[5], Makoto Sunamori[2], John M Sedivy[4] and Shigetaka Kitajima[1,*]

[1]Department of Biochemical Genetics, Medical Research Institute and Laboratory of Genome Structure and Regulation, School of Biomedical Science, Tokyo Medical and Dental University, Yushima, Bunkyo-ku, Tokyo, Japan,[2]Department of Cardiothoracic Surgery, Tokyo Medical and Dental University, Yushima, Bunkyo-ku, Tokyo, Japan, [3]Department of Cardiovascular Medicine, Tokyo Medical and Dental University, Yushima, Bunkyo-ku, Tokyo, Japan, [4]Department of Molecular Biology, Cell Biology, and Biochemistry, Brown University, Providence, RI, USA and [5]Division of Neurofunctional Genomics, Department of Immunobiolgy and Neuroscience, Medical Institute of Bioregulation, Kyushu University, Maidashi, Higashi-ku, Fukuoka, Japan

The c-*myc* proto-oncogene encodes a transcription factor that promotes cell cycle progression and cell proliferation, and its deficiency results in severely retarded proliferation rates. The *ATF3* stress response gene encodes a transcription factor that plays a role in determining cell fate under stress conditions. Its biological significance in the control of cell proliferation and its crosstalk regulation, however, are not well understood. Here, we report that the serum response of the *ATF3* gene expression depends on c-*myc* gene and that the c-Myc complex at ATF/CREB site of the gene promoter plays a role in mediating the serum response. Intriguingly, ectopic expression of ATF3 promotes proliferation of c-*myc*-deficient cells, mostly by alleviating the impeded G1-phase progression observed in these cells, whereas ATF3 knockdown significantly suppresses proliferation of wild-type cells. Our study demonstrates that ATF3 is downstream of the c-Myc signaling pathway and plays a role in mediating the cell proliferation function of c-Myc. Our results provide a novel insight into the functional link of the stress response gene *ATF3* and the proto-oncogene c-*myc*.

The EMBO Journal (2005) **24**, 2590–2601. doi:10.1038/sj.emboj.7600742; Published online 30 June 2005
Subject Categories: chromatin & transcription; cell cycle
Keywords: ATF3; c-Myc; cell cycle progression; crosstalk

Introduction

The c-*myc* proto-oncogene regulates cell growth, proliferation, differentiation, and apoptosis, and its deregulation is implicated in the development of numerous human cancers (Henriksson and Luscher, 1996). Since c-Myc is a transcription factor and its expression is induced by serum and a variety of mitogens, it is important to identify its targets or the modulator gene(s) that mediate its effect on cell proliferation. Recently, several studies have used microarray analysis to compare Myc-driven changes in global gene expression. These studies have revealed that candidate c-Myc target genes fall into a broad spectrum of diverse functional categories, ranging from metabolic enzymes, biosynthesis of macromolecules such as RNA, protein and DNA, transcription, and cell signaling (Menssen and Hermeking, 2002; Fernandez *et al*, 2003; O'Connell *et al*, 2003). The target genes identified in these studies with respect to cell cycle control partially overlap but there are also non-overlapping outliers, perhaps stemming from the different assay systems used in controlling c-Myc expression. Thus, our knowledge of the functional link between c-*myc*'s role in cell proliferation and those target genes is still limited.

Homozygous deletion of the c-*myc* gene in mice leads to numerous developmental abnormalities and embryonic lethality at 10.5 days of gestation (Davis *et al*, 1993). Studies using conditional mutations or incremental reduction of c-Myc expression have shown that c-Myc is required to maintain the proliferation of embryonic fibroblasts, or to regulate the percentage of cells that re-enter the cell cycle (de Alboran *et al*, 2001; Trumpp *et al*, 2001). By contrast, a homozygous c-*myc* knockout in a rat fibroblast cell line is not lethal but results in a severely retarded cell growth phenotype, mainly due to lengthening of the G1 phase (Schorl and Sedivy, 2003). This culture model of c-*myc* knockout has been used extensively to investigate the roles of c-*myc* and its related target genes in the regulation of cell cycle progression. For instance, cyclin-dependent kinase 4 (CDK4) has been shown to partially restore the proliferation defect of c-*myc*-deficient cells (Hermeking *et al*, 2002). Effectors of the c-Myc signaling pathway and its crosstalk in cell proliferation, however, are still largely unknown.

The stress-inducible transcription factor ATF3 is a member of the ATF/CREB family of basic leucine zipper (b-Zip) type transcription factors. It is induced upon exposure of cells to a variety of physiological and pathological stimuli (Hai *et al*, 1999, and references therein). The stress response of ATF3 is mediated through the c-Jun N-terminal kinase (JNK) mitogen-activated protein kinase (MAPK) or through a p53-dependent pathway, and stabilization of its mRNA is one mechanism for the control of the rapid induction of ATF3 in HeLa cells treated with anisomycin (Liang *et al*, 1996). This response is thought to have detrimental effects on the cell, such as cell cycle arrest and apoptosis (Yin *et al*, 1997; Hai *et al*, 1999; Cai *et al*, 2000; Kang *et al*, 2003). On the other hand, *ATF3* is also rapidly induced in regenerating liver (Hsu *et al*, 1991), or in cells treated with growth-stimulating factors such as serum, epidermal growth factor, or fibroblast growth factor (Mohn *et al*, 1991; Iyer *et al*, 1999). ATF3 partially

*Corresponding author. Department of Biochemical Genetics, Laboratory of Gene Structure and Regulation, Tokyo Medical and Dental University, 1-5-45 Yushima, Bunkyo-ku, Tokyo 113-8510, Japan.
Tel.: +81 3 5803 5822; Fax +81 3 5803 0248;
E-mail: kita.bgen@mri.tmd.ac.jp

Received: 12 January 2005; accepted: 13 June 2005; published online: 30 June 2005

transforms chick embryo fibroblasts by promoting growth factor-independent proliferation (Perez *et al*, 2001), and induces DNA synthesis and expression of cyclin D1 in hepatocytes (Allan *et al*, 2001). Recently, we have reported that ATF3 supports cell survival by downregulating p53 transcription in endothelial and cardiac cells (Kawauchi *et al*, 2002; Nobori *et al*, 2002). ATF3 also protects neuronal cells from JNK-induced cell death by inducing heat shock protein 27 and Akt activation (Nakagomi *et al*, 2003). These data support a role for *ATF3* in cell proliferation and survival. The transcriptional mechanism and biological significance of *ATF3* expression in response to growth stimuli, however, remain elusive.

Here we report that serum response of the *ATF3* gene depends on *c-myc* gene status and that the retarded cell proliferation phenotype of c-*myc*-deficient cells is partially but significantly restored by ectopic expression of ATF3. This study demonstrates for the first time that ATF3 functionally interacts with the c-Myc signaling pathway, providing a novel insight into the functional coordination between cell cycle control and stress response.

Results

Serum induction of ATF3 is abrogated in c-myc-deficient cells

ATF3 has been shown to be rapidly induced in response to partial hepatectomy in the rat (Hsu *et al*, 1991) or after serum treatment of HeLa cells and fibroblasts (Mohn *et al*, 1991; Iyer *et al*, 1999). We first serum-starved wild-type and c-*myc*-deficient HO15.19 rat fibroblasts for 48 h, and then stimulated them with serum. ATF3 mRNA was induced in wild-type cells, reaching a maximum level at 3 h after stimulation, whereas ATF3 protein was induced 3 h after stimulation with a peak at 6–12 h (Figure 1A). This rapid induction of ATF3 mRNA may partly be due to its increased stability, as reported (Liang *et al*, 1996). Under this condition, the c-*myc* mRNA and protein were more rapidly induced than ATF3, and reached their maximum levels at 1 and 3 h after serum treatment, respectively. In c-*myc*-deficient cells, on the other hand, ATF3 expression was almost completely abrogated at both the mRNA and protein levels (Figure 1A). ATF3 was induced in response to serum at levels similar to wild-type cells in both c-*myc* heterozygous cells and c-*myc* homozygous cells reconstituted with a c-*myc* transgene (Figure 1B), indicating that the serum induction of ATF3 gene depends on c-*myc* gene status. We next treated wild-type and c-*myc*-deficient cells with UV and etoposide, since ATF3 is also induced in response to various cytotoxic stimuli through JNK/MAPK pathway, or p53-dependent and -independent pathways (Yin *et al*, 1997; Hai *et al*, 1999; Cai *et al*, 2000). ATF3 was induced by these stress stimuli in both cell types at similar levels (Figure 1C), indicating that the signaling pathway(s) of ATF3 stress response to UV and etoposide is not c-Myc dependent.

Serum induction of ATF3 is mediated by the ERK/MAPK pathway

Serum treatment causes a rapid phosphorylation of extracellular signal-regulated kinase (ERK) and eventually leads to the activation of its target gene promoters. We thus examined the effect of PD98059, a specific MEK1 kinase inhibitor that

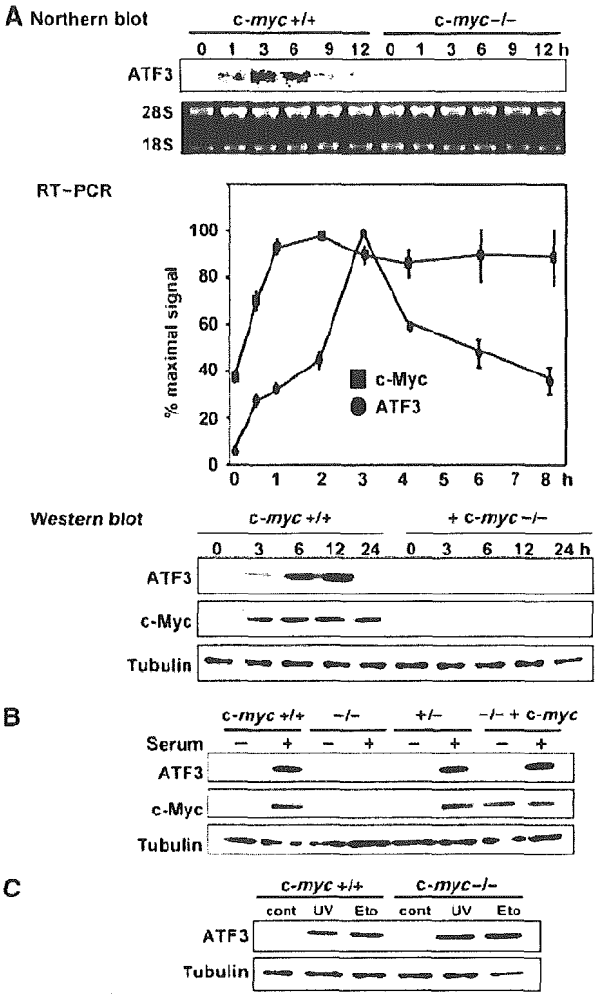

Figure 1 Serum induction of ATF3 in c-*myc*-deficient cells. (**A**) Upper panel: Northern blot analysis of ATF3 mRNA in serum-stimulated wild-type TGR1 and c-*myc*-deficient HO15.19 cells. Middle panel: RT-PCR analysis of ATF3 and c-Myc mRNA in wild-type cells after serum stimulation. Results are means with s.d. of triplicate experiments and shown as percent of the maximal amount of each transcript. Lower panel: Western blot analysis of ATF3 and c-Myc in wild-type and c-*myc*-deficient cells after serum stimulation. Immunoblot of tubulin is shown as a control of protein loading. (**B**) Western blot analysis of ATF3 and c-Myc in heterozygous c-*myc*-knockout +/− cells and homozygous c-*myc*-knockout −/− cells reconstituted with a c-*myc* transgene after serum stimulation. Cell extracts were prepared 12 h after serum treatment. (**C**) Stress-induced expression of ATF3 in wild-type and c-*myc*-deficient cells in response to UV (40 J/m^2) or 20 μM etoposide (Eto). Control (cont) represents untreated cells.

suppresses the phosphorylation of ERK, on ATF3 induction. PD98059 almost completely abolished the serum induction of ATF3, whereas JNK inhibitor SP600125 or p38 inhibitor SB203580 had no significant effect. This indicates that the activation of MEK1/ERK is essential for the serum-induced expression of ATF3 (Figure 2A). Serum treatment caused rapid phosphorylation of ERK with similar kinetics in both wild-type and c-*myc*-deficient cells (Figure 2B), in agreement with a previous report (Mateyak *et al*, 1999). These data strongly suggest that serum induction of ATF3 is impaired downstream of the ERK/MAPK activation in c-*myc*-deficient cells.

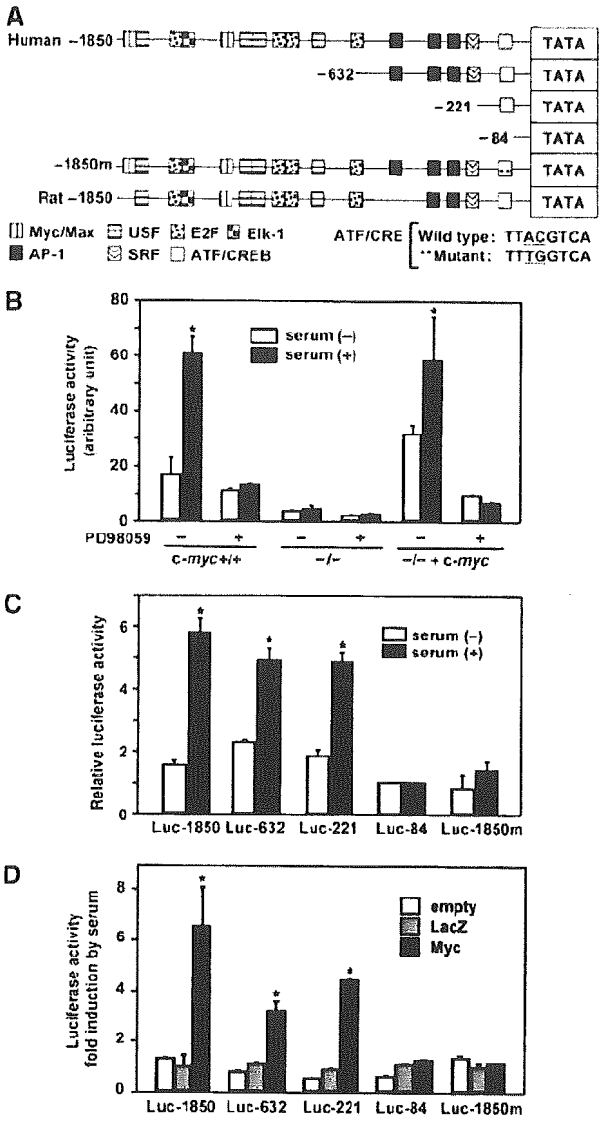

Figure 3 Repression of serum-induced ATF3 reporter activity in c-*myc*-deficient cells. (**A**) Human and rat ATF3 gene promoters with putative consensus elements for ATF/CREB, AP1, c-Myc/USF, and other factors are aligned (Liang *et al*, 1996). Human ATF3 reporter plasmids containing various deletions or two point mutations of ATF/CRE site are also depicted. (**B**) Serum induction of ATF3 promoter activity was assayed in wild-type TGR1 cells using pATF3Luc1850 in the presence or absence of 25 μM PD98059 for 24 h. Results are mean ± s.d. of triplicate assays. Significant induction by serum compared with control, $^*P<0.05$. (**C**) Wild-type cells were transfected with ATF3 reporters containing various deletions or ATF/CRE point mutations, and assayed for serum induction. Relative activity to that of minimal promoter pATF3Luc-84 was the mean with s.d. of triplicate experiments. Significant induction by serum compared with control, $^*P<0.05$. (**D**) c-*myc*-deficient cells were transfected with various reporter plasmids along with empty, LacZ or c-Myc expression vectors and treated with 10% serum. Fold induction by serum is shown and represents the mean with s.d. of triplicate experiments. Significant induction by c-Myc compared with control, $^*P<0.05$.

examine the *in vivo* recruitment of these factors to the ATF3 gene promoter. Both anti-ATF2 and anti-c-Jun antibodies immunoprecipitated the proximal region of the ATF3 gene promoter from −120 to +30, containing the ATF/CRE motif, in both serum-starved and serum-stimulated cells, whereas control IgG did not (Figure 4B). The anti-c-Myc antibody also immunoprecipitated the proximal promoter region after serum treatment, while it immunoprecipitated very little, if any, of this region in serum-starved cells. When ChIP assay was performed using an anti-ATF2 or an anti-c-Jun antibody, the promoter region was less efficiently immunoprecipitated in c-*myc*-deficient cells than in wild-type cells, indicating that ATF2/c-Jun binding is c-Myc dependent. In the light of these results, we conclude that ATF2 and c-Jun become activated to bind to the ATF/CRE motif *in vivo*, and c-Myc is also recruited to this region of *ATF3* in response to serum.

c-Myc associates with ATF2/c-Jun complex both in vivo and in vitro

To determine the nature of c-Myc recruitment to the proximal region of *ATF3* gene promoter, we performed an immunoprecipitation assay using cells overexpressing c-Myc, ATF2, and c-Jun. As illustrated in Figure 4C (see also Supplementary Figure S2), both anti-ATF2 and anti-c-Jun antibodies specifically immunoprecipitated the ATF2/c-Jun complex. Under this condition, c-Myc protein was also co-precipitated by these antibodies, but not by control IgG. When the assay was performed with anti-c-Myc antibody, both ATF2 and c-Jun were co-precipitated, clearly indicating that c-Myc, ATF2, and c-Jun form a complex *in vivo*. To address whether c-Myc directly interacts with ATF2/c-Jun complex, an *in vitro* binding assay was performed using recombinant GST-c-Myc, ATF2, and c-Jun proteins. c-Myc was capable of binding to ATF2, while it formed very little, if any, complex with c-Jun (Figure 4D, left panel). This was also observed when the mixture was inversely immunoprecipitated with an anti-ATF2 or an anti-c-Jun antibody (Figure 4D, right panel). In contrast, when GST-c-Myc was mixed with ATF2 and c-Jun together, c-Myc bound to ATF2/c-Jun complex (Figure 4D, left lower panel). These data suggest that c-Myc forms a ternary complex with ATF2/c-Jun through its direct binding to ATF2.

Expression of ATF3 promotes cell cycle progression in c-myc-deficient cells

Homozygous deletion of the c-*myc* gene in rat fibroblasts significantly impedes G1-phase progression and results in the severe retardation of cell proliferation rates (Schorl and Sedivy, 2003). Since our data indicate that *ATF3* is induced downstream of c-*myc*, we overexpressed the ATF3 protein in c-*myc*-deficient cells to test whether ATF3 can rescue their proliferation defect. We first employed adenovirus-mediated gene transfer to control the duration and amount of ATF3 expression such that it mimics the *in vivo* serum induction of *ATF3*. As illustrated in Figure 5A, ATF3 promoted the proliferation of c-*myc*-deficient cells, while LacZ expression had no effect. By contrast, ATF3 exerted only a marginal effect on the proliferation of wild-type cells. The level of ATF3 expression at 25 MOI was comparable to that observed in serum-induced wild-type cells while at 50 MOI it was two-to three-fold higher (Figure 5B), indicating that the expression of ATF3 at physiological amounts exerts cell proliferation activity. In the absence of serum, however, ATF3 was not capable of promoting cell proliferation. We also performed retrovirus gene transfers and established c-*myc*-deficient cell lines stably expressing ATF3 to examine the effect of ATF3 in a long-term assay. As in Figure 5C, these cell lines proliferated faster

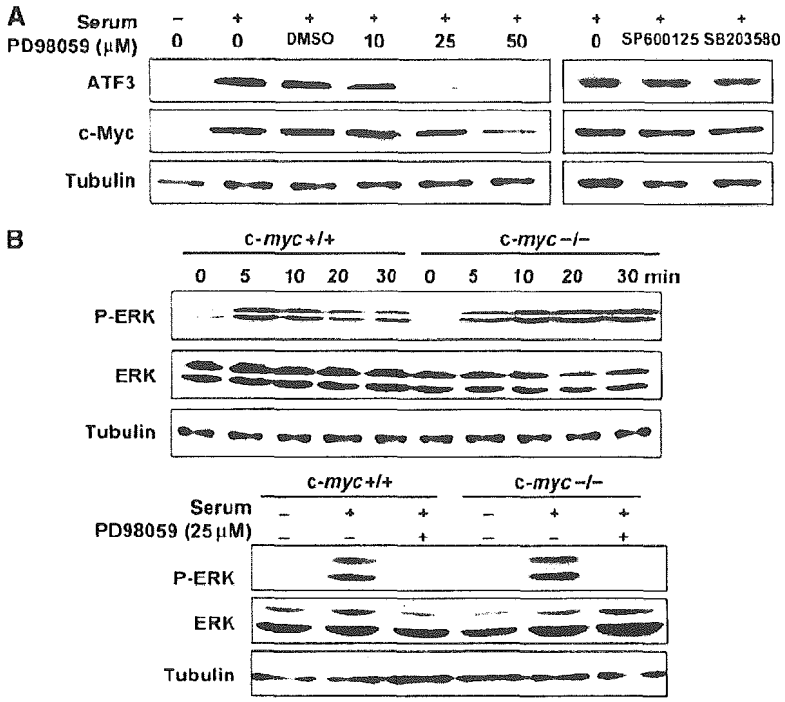

Figure 2 Serum-induced expression of ATF3 via ERK/MAPK signaling pathway. (**A**) Effect of MAPK inhibitors on serum-induced ATF3 expression in wild-type TGR1 cells determined by Western blot. The inhibitors were added 2 h before adding serum, and cell extracts were prepared 12 h after serum treatment. *SP600125* and *SB203580* were used at 10 and 25 μM, respectively. DMSO indicates vehicle only. (**B**) Phosphorylated ERK (P-ERK) and ERK (ERK) were measured at the indicated time after serum treatment of wild-type and c-*myc*-deficient cells by Western blot. Both 42 and 44 kDa isoforms were detected. In the lower panel, the activity 10 min after serum treatment in the presence of 25 μM PD98059 is shown.

Serum induction of ATF3 promoter activity is suppressed in c-myc-deficient cells

To determine whether the c-*myc*-dependent serum induction of *ATF3* is regulated at the level of transcription, we performed an ATF3 gene reporter assay. Figure 3A illustrates the putative promoter elements of the *ATF3* gene promoter, including c-Myc/Max binding sites as well as consensus motifs mediating the serum response (Liang *et al*, 1996), which are highly conserved between human and rat. As can be seen in Figure 3B, the *ATF3* promoter was activated 3.8-fold in wild-type cells after serum treatment, and this activation was suppressed in the presence of PD98059. On the other hand, basal promoter activity in c-*myc*-deficient cells in the absence of serum was one-fifth the level of wild-type cells, and its induction by serum was significantly abrogated with only 1.1- to 1.3-fold activation. Both the basal and serum-induced promoter activities were fully restored in HO/myc3 cells containing the c-*myc* transgene. We next measured *ATF3* promoter activity in wild-type cells using various deletion mutants. The deletion constructs down to −221 were all induced by serum (Figure 3C). In contrast, a further deletion down to −84 almost completely abolished serum induction. Since the region between −221 and −84 contains the putative ATF/CRE motif at −92 to −85, we performed the assay using the pLucATF3-1850m containing two point mutations at the ATF/CRE site (Cai *et al*, 2000). This mutation caused a marked reduction of serum-induced activity (Figure 3C). We next examined serum response of the reporter after expressing c-Myc protein in c-*myc*-deficient cells. c-Myc expression restored the serum response of pLucATF3-1850, -632, and -221, but had no effect on that of pLucATF3-84 and -1850m (Figure 3D), whereas control or LacZ expression had no effect. Combined, these results indicate that the ATF/CRE site in the *ATF3* gene promoter represents one of the major elements responsible for the c-Myc-dependent serum response of *ATF3*.

ATF2/c-Jun complex binds the ATF/CRE motif and c-Myc is recruited to the proximal region of the ATF3 promoter

We next performed a gel mobility shift assay using the ATF/CRE motif as a DNA probe. Incubation of probe with nuclear extracts from serum-starved cells produced bands over a broad size range (Figure 4A). These bands were specific for the ATF/CRE site, since assays in the presence of a wild-type cold probe but not mutant probe completely abolished their formation (data not shown; Cai *et al*, 2000). The intensity of these bands in serum-stimulated cells was significantly higher than in serum-starved cells. In supershift assays using various antibodies, both anti-ATF2 and anti-c-Jun antibodies resulted in supershifts, indicating that they are components of the protein–DNA complex (Figure 4A). Antibodies against ATF3, ATF4, CREB, JunB, or JunD did not result in any apparent supershifts (data not shown). Anti-c-Myc antibody decreased the intensity of the bands formed. The data indicate that ATF2 and c-Jun are induced to bind to the ATF/CRE motif in response to serum, and c-Myc might be involved in the complex formation (see also Supplementary Figure S1). To further investigate this possibility, we performed a chromatin immunoprecipitation (ChIP) assay to

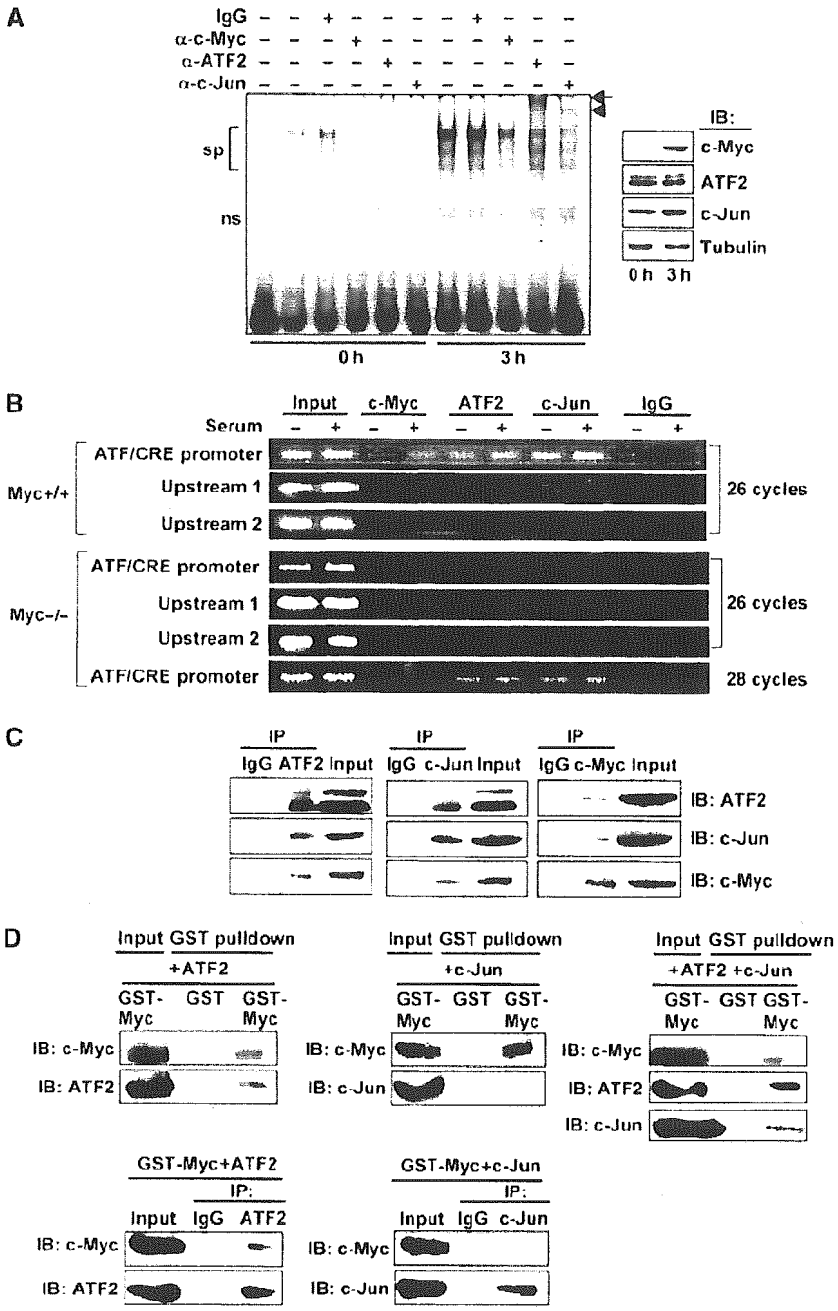

Figure 4 Binding of ATF2/c-Jun to ATF/CRE motif and c-Myc recruitment to the *ATF3* gene promoter in response to serum. (**A**) Nuclear extract from wild-type cells serum starved or serum stimulated for 3 h was assayed for gel shift using radiolabeled DNA probe from −102 to −73 containing the ATF/CRE motif. From left: probe only, extract from the starved or serum-stimulated cells with or without the indicated antibodies. sp: specific bands; ns: nonspecific bands; arrow: supershift by anti-ATF2 antibody; arrowhead: supershift by anti-c-Jun antibody. In the inset, the expressions of c-Myc, ATF2, and c-Jun proteins were measured by Western blot. (**B**) Upper panel: Serum-starved or serum-stimulated wild-type cells were crosslinked with formaldehyde, and ChIP assay was performed using anti-c-Myc, anti-ATF2, or anti-c-Jun antibodies. ATF/CRE promoter region from −120 to +30, upstream region 1 from −370 to −120, and upstream region 2 from −570 to −370 were amplified by 26 cycles of PCR. Lower panel: c-*myc*-deficient cells were also subjected to ChIP assay, as above. ATF/CRE promoter region was also amplified by 28 cycles of PCR. (**C**) Whole-cell extracts from 293T cells overexpressing c-Myc, ATF2, and c-Jun were immunoprecipitated as in Materials and methods using anti-ATF2 (left panel), anti-c-Jun (middle panel), or anti-c-Myc antibody (right panel), respectively, and the resulting immune complex was subjected to Western blot analysis. Input was 10% of total. (**D**) Recombinant GST-c-Myc was mixed with ATF2 (upper left panel) or c-Jun alone (upper middle panel), or together (upper right panel), and GST pulldown assay was performed as in Materials and methods. In the lower panel, binding of GST-c-Myc with ATF2 or c-Jun was inversely assayed by immunoprecipitation using anti-ATF2 (lower left panel) or anti-c-Jun antibody (lower right panel), respectively. Input was 10% of total.

compared to their parent cells. Moreover, the A2 cell line expressing ATF3 at an amount higher than A1 displayed a higher proliferation rate. A1 cells displayed a roughly circular outline with occasional long processes as parental c-*myc*-deficient HO15 cells (Mateyak *et al*, 1997), demonstrating that the ATF3 expression causes no significant alteration of

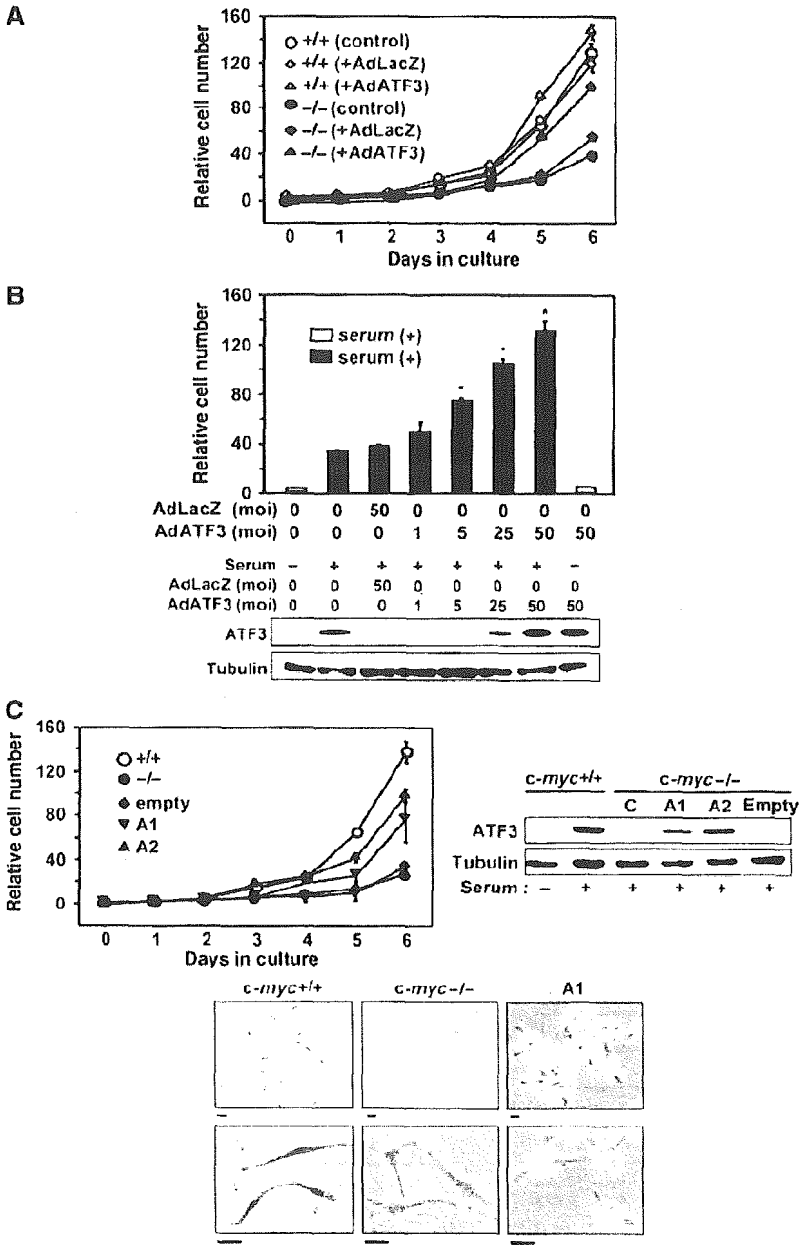

Figure 5 Proliferation of c-*myc*-deficient cells by ectopic expression of ATF3. (**A**) Wild-type and c-*myc*-deficient cells were infected with AdATF3 or AdLacZ at 25 MOI for 48 h and their proliferation rates were assayed. Relative cell number is shown as mean±s.d. of triplicate assays. (**B**) Dose-dependent cell proliferation by ATF3 in c-*myc*-deficient cells. Significant proliferation by ATF3 compared with control, $^*P<0.05$. The lower panel shows the ATF3 expression in AdATF3-infected cells. In the left two lanes, the level of ATF3 expression in serum-stimulated wild-type cells is also shown. (**C**) Upper left panel: Proliferation rates of the c-*myc*-deficient cell lines A1 and A2 stably expressing ATF3. The relative cell numbers are the mean±s.d. of triplicate assays. Significant cell proliferation in A1 and A2 compared with control, $^*P<0.05$. The upper right panel shows the ATF3 expression in A1 and A2 cells. Lower panel: Morphology of wild-type, c-*myc*-deficient, and A1 cells is shown. Scale bar, 20 μm.

cell shape. Taken together, these results clearly indicate that ATF3 is capable of promoting the proliferation of c-*myc*-deficient cells.

Cell cycle promoters are upregulated and G1-phase progression defect is alleviated by ATF3 in c-myc-deficient cells

To assess the effect of ATF3 on cell cycle progression, we measured Cdk4 and Cdk2 activities in c-*myc*-deficient cells exogenously expressing ATF3. While LacZ expression had no effect, ATF3 expression resulted in increased kinase activity by both Cdk4 and Cdk2, providing biochemical evidence that ATF3 promotes cell cycle activation (Figure 6A). Next, we synchronized these cells at G0 by serum starvation, and examined the expression of various cell cycle regulators after stimulating them with serum. As illustrated in Figure 6B, the expressions of cyclins D1, E, and A, and Cdk2 and Cdk4 were all upregulated in these cells compared

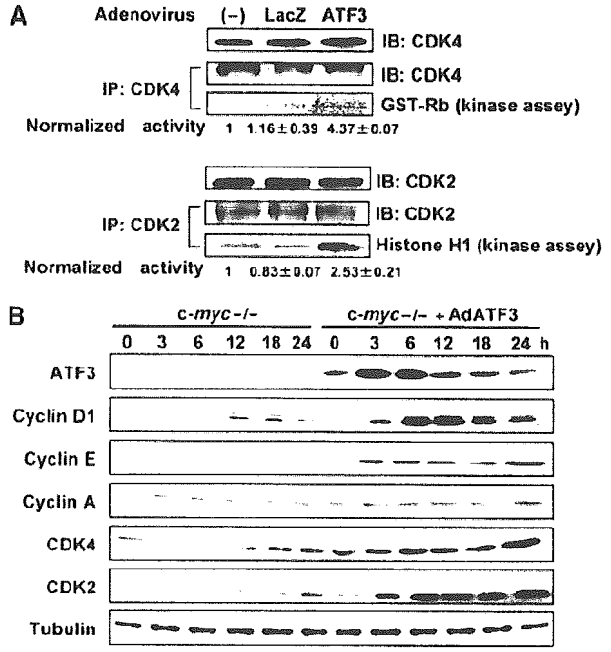

Figure 6 Effect of ATF3 on Cdk activity and the expression of various cell cycle regulators. (**A**) Cdk4 and Cdk2 kinase activities of c-*myc*-deficient cells treated with AdATF3 and serum for 48 h were assayed from lysates of exponentially growing cells, as previously reported (Tamamori-Adachi *et al*, 2004). The activities were normalized to the amount of Cdk4 and Cdk2. (**B**) Cell cycle regulators were measured by Western blot analysis at each time point after serum stimulation of c-*myc*-deficient cells infected with AdLacZ or AdATF3 (25 MOI) for 48 h. Immunoblots of tubulin are shown as control.

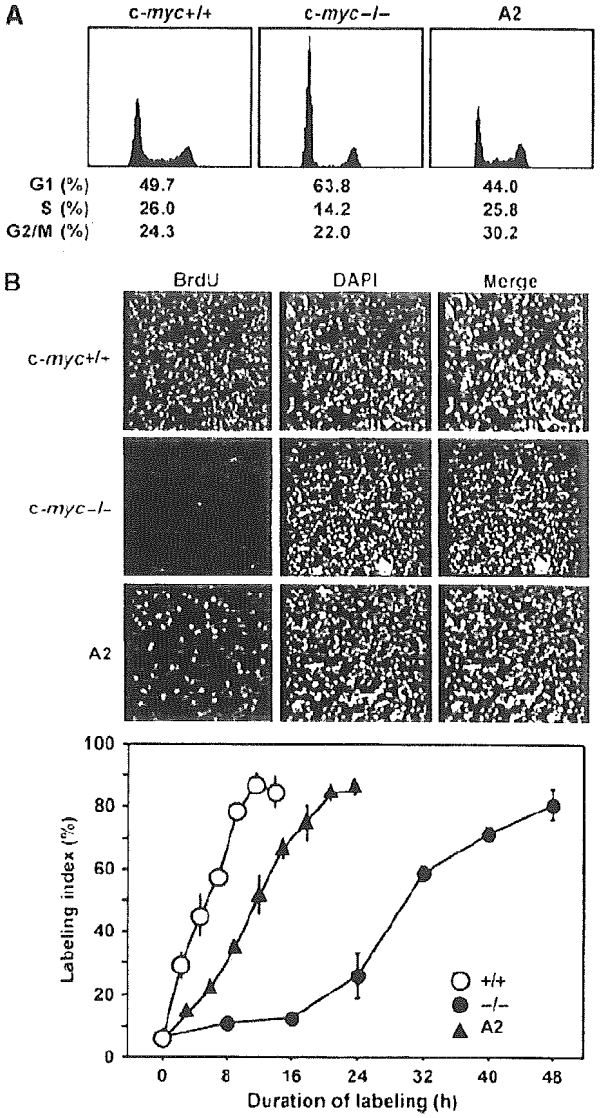

Figure 7 Effect of ATF3 on the cell cycle of c-*myc*-deficient cells. (**A**) Asynchronously cycling wild-type, c-*myc*-deficient, and A2 cells stably expressing ATF3 were analyzed by FACS as in Materials and methods. (**B**) Each cell line was synchronized by mitotic shake-off in M phase and continuously labeled with 10 μM BrdU as in Materials and methods. Upper panel: Representative data of *in situ* immunostaining of BrdU-positive cells after 8 h labeling. DAPI denotes nuclear staining. Lower panel: At the indicated time points, BrdU-positive cells were measured by histochemical staining and the percentage of BrdU-positive cells was scored as labeling index. At least 700 cells were scored at each time point.

to control LacZ-expressing cells. We then examined cell cycle progression by flow cytometry. As shown in Figure 7A and Table I (see also Supplementary Figure S3 and Supplementary Tables 1 and 2), the percent cell cycle distribution and the G1-phase duration of c-*myc*-deficient cells were significantly restored in A2 cells, which stably express ATF3, although S and G2/M phases were less affected. To assess cell cycle profile more accurately, we pulse-labeled the A2 cells with 5-bromodeoxyuridine (BrdU) and corrected the fluorescence-activated cell sorting (FACS) data as in Table I. The result supports a rather selective restoration of G1-phase duration in A2 cells. Alternatively, A2 cells were synchronized in M phase by mitotic shake-off and labeled with BrdU. The cells displayed significantly enhanced incorporation of BrdU and exhibited a shortened G1 phase of 11.7 h, compared to 30.4 h of parental c-*myc*-deficient cells (Figure 7B and Table I). Overall, ATF3 expression significantly decreased the duration of the cell cycle of c-*myc*-deficient cells from 46.8 to 26.8 h in A2 cells. These data indicate that ATF3 alleviates the inhibition of cell cycle progression in c-*myc*-deficient cells by upregulating various cell cycle regulators and selectively augmenting the G1-phase progression of the cell cycle.

Serum-induced cell proliferation is inhibited by knockdown of ATF3

We next addressed whether ATF3 is implicated in serum-induced cell proliferation of wild-type cells by employing a loss-of-function approach via an RNA interference-mediated gene knockdown. We isolated wild-type TGR1 cell lines stably expressing siRNAs for ATF3, starved these cells for 48 h, and then stimulated with 10% serum. As illustrated in Figure 8A, ATF3 induction by serum was significantly suppressed in cell lines #1 and #2, while c-Myc induction was not affected. The proliferation of these cells was significantly suppressed compared with control cells (Figure 8B). Moreover, various deletions of ATF3 had inhibitory effect on the proliferation of wild-type cells, possibly acting in a dominant-negative manner (see Supplementary Figure S4). These data clearly indicate that *ATF3* plays a crucial role in supporting cell proliferation in response to serum.

Table I Cell cycle parameters of wild, c-*myc*−/−, and A2 cells

	c-*myc*+/+			−/−			A2		
	G1	S	G2/M	G1	S	G2/M	G1	S	G2/M
Cell cycle phase (h)[a]	9.2	4.8	4.6	29.9	6.6	10.3	11.8	6.9	8.1
Total doubling time (h)[b]		18.6			46.8			26.8	
Cell cycle distribution (%)[c]	33.4	58.6	8	56.7	28.4	14.9	37.3	39.2	23.5
Cell cycle phase (h)[d]	6.2	10.9	1.5	26.5	13.3	7.0	10.0	10.5	6.3
Mitotic shake-off (h)[e]	4.6			30.4			11.7		

[a]Cell cycle phase was calculated from cell cycle distributions based on flow cytometric analysis.
[b]Doubling time was calculated from cell cycle distributions based on growth rates.
[c]Cell cycle distributions shown in Figure 7A were corrected using BrdU incorporation values of 58.6% (c-*myc*+/+ cells), 28.4% (c-*myc*−/− cells), and 39.2% (A2 cells), respectively. These values were determined by pulse labeling of BrdU as in Materials and methods.
[d]Corrected cell cycle distributions were combined with growth rate values (doubling time).
[e]G1 phase duration from data in Figure 7B. Values for 50% labeling index are shown.

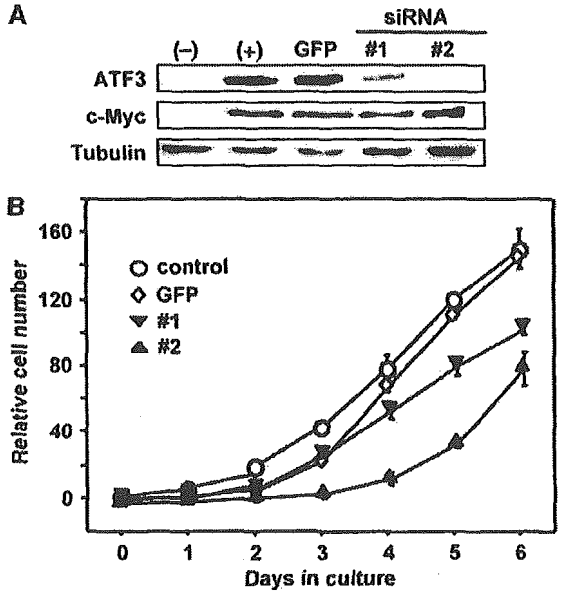

Figure 8 Effect of ATF3 knockdown on proliferation activity of wild-type cells. (**A**) TGR1 cell lines #1 and #2 stably expressing ATF3 siRNA were established as in Materials and methods. The cells were serum starved for 48 h and stimulated with 10% serum for 8 h, and their expression of ATF3 and c-Myc was assayed by Western blot. TGR1 cell line stably expressing GFP siRNA was used as control. (**B**) Proliferation of ATF3 siRNA #1, #2, and GFP siRNA cell lines was determined as in Materials and methods.

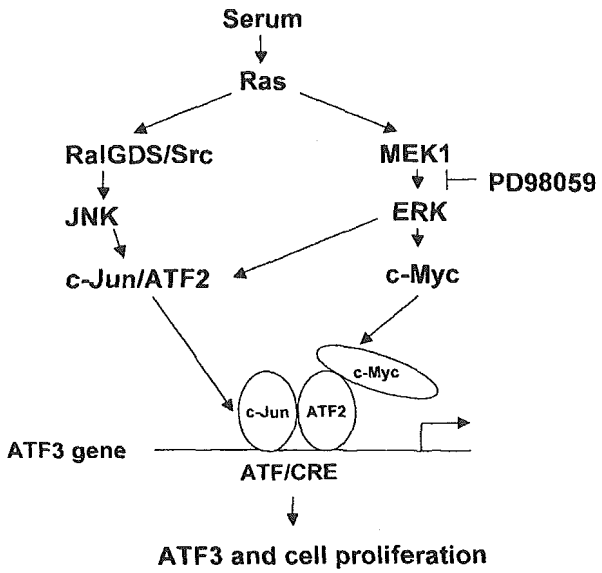

Figure 9 A crosstalk model of *ATF3* and c-*myc* in serum induction. Serum induces c-Myc and ATF2 through MEK1–ERK pathway, and also c-Jun by RALGDS/Src–JNK pathway (de Ruiter *et al*, 2000; Ouwens *et al*, 2000). These factors form complex at or around the ATF/CRE motif of *ATF3* gene promoter, and thereby activate *ATF3* gene expression. Expressed ATF3 protein functions as a positive regulator of cell cycle and mediates cell proliferative activity of c-Myc.

Discussion

The stress response gene *ATF3* is induced by various stress stimuli and its activation is associated with cell death (Yin *et al*, 1997; Hai *et al*, 1999; Cai *et al*, 2000, Kang *et al*, 2003), survival (Kawauchi *et al*, 2002; Nobori *et al*, 2002; Nakagomi *et al*, 2003), and cell proliferation (Hsu *et al*, 1991; Mohn *et al*, 1991; Iyer *et al*, 1999; Allan *et al*, 2001; Perez *et al*, 2001). Thus, ATF3 can function differently depending on cellular context. In this study, we have demonstrated that ATF3 is induced downstream of the c-Myc signaling pathway and plays a crucial role in mediating cell proliferative activity of c-Myc during serum response.

Using rat c-*myc*-deficient cells, we have shown that ATF3 is induced downstream of the c-Myc signaling pathway in response to serum, as illustrated in our model in Figure 9. This is supported by the following results: (1) *ATF3* mRNA and protein were induced at times later than those of c-*myc* (Figure 1A); (2) *ATF3* induction was abrogated in c-*myc*-deficient cells, and reconstituting these cells with the c-*myc* transgene restored the serum response (Figure 1A and B); and (3) serum induction of ATF3 reporter activity was severely repressed in c-*myc*-deficient cells, while coexpression of reporter with c-Myc restored activity (Figure 3). In contrast, *ATF3* induction by DNA damage was not c-Myc dependent, suggesting that c-Myc might not be significantly involved in p53-dependent or -independent stress response of ATF3 (Fan *et al*, 2002; Zhang *et al*, 2002).

Induction of ATF3 was previously shown to be mediated, at least in part, by increased stability of the message in anisomycin-treated HeLa cells (Liang *et al*, 1996), whereas TNFα-mediated induction of ATF3 mRNA, but not its stabi-

lity, is regulated by the JNK and ERK pathways in vascular endothelial cells (Inoue *et al*, 2004). In this study, we have further demonstrated that the serum induction of ATF3 is also regulated at transcription level, and ATF/CRE motif of the *ATF3* gene promoter plays a role in its serum-dependent and c-Myc-dependent activation. In both gel shift and ChIP assays, the ATF2/c-Jun complex was already bound to the ATF/CRE motif in the absence of serum but its binding was significantly enhanced after serum treatment (Figure 4). This is consistent with the idea that the factors bound to the motif are not activated prior to serum treatment, but activated via ERK MAPK after serum stimulation. It has in fact been demonstrated that ATF2 and c-Jun are activated through this pathway in serum-treated cells (de Ruiter *et al*, 2000; Ouwens *et al*, 2000), and the coexpression of ATF2 and c-Jun activates the ATF3 promoter, supporting synergistic action of these factors (Liang *et al*, 1996). c-Myc was involved in the serum-dependent activation of the *ATF3* gene, most likely independent of DNA binding, since c-Myc conferred serum response on the pLuc-221 reporter that contains an ATF/CRE site but no apparent E box (Figure 3D). c-Myc was recruited to the proximal promoter region of the *ATF3* gene after serum stimulation, and this region, from −120 to +30, does not contain any putative E boxes or other sequences for c-Myc's recruitment such as YY-1 (Shrivastava *et al*, 1996), SP1, Ap2, or Miz-1 sites (Sakamoto and Prendergast, 1999). Thus, we speculate that the ternary complex of ATF2/c-Jun/c-Myc is formed at or around the ATF/CRE site. This is supported by our data demonstrating that c-Myc interacted with ATF2/c-Jun both *in vivo* and *in vitro* (Figure 4C and D). This complex may be recruited to the chromatin remodeling complex or the RNA polymerase II initiation complex, thereby mediating the serum response in a concerted action with ATF2 and c-Jun. Indeed, SWI/SNF (Cheng *et al*, 1999; McMahon *et al*, 2000) and some general transcription factors such as TBP and pTEFb (Eberhardy and Farnham, 2001) have been reported to interact with c-Myc. However, the molecular mechanism by which c-Myc activates the *ATF3* gene in response to serum currently remains unclear. It should be noted that the c-Myc protein is stabilized by the phosphorylation of its serine 62 residue by the MAPK/ERK signaling pathway (Sears *et al*, 1999; Sears *et al*, 2000). This rapid stabilization of c-Myc along with its transcriptional induction may act to efficiently induce *ATF3* during the initial stage of cell proliferation. In this study, we could not determine the significance of the binding sites for c-Myc, E2F, SRF, or AP1 in the ATF3 promoter, although the deletion of these sites slightly reduced the serum response of the reporter when the activity of pLuc-1850 was compared with that of pLuc-632 (Figure 3C). Further studies are needed to understand the significance of these sites in serum response.

More intriguingly, ATF3 significantly promoted the proliferation of c-*myc*-deficient cells that otherwise display a severe retardation of cell cycle progression. This effect of ATF3 may have a role *in vivo* since enhanced cell proliferation was observed by expression of ATF3 at physiological levels (Figure 5). Furthermore, knockdown of ATF3 by siRNA (Figure 8) or expression of deletion mutants of ATF3 (Supplementary Figure S4) strongly inhibited serum-induced cell proliferation. ATF3 restored the delayed progression of G1 phase in c-*myc*-deficient cells, as determined by flow cytometry and BrdU labeling (Figure 7 and Table I), and induced the expression of cyclins D1, A, and E, and activated CDK2 and CDK4 (Figure 6). In this regard, it has been shown that cyclin D1 is transcriptionally induced by ATF3 (Allan *et al*, 2001), which suggests that ATF3 induces cyclin D1, which in turn cooperates with CDK4 to promote G1-phase progression. Furthermore, CDK4 has been shown to be a direct target of c-*myc*, and overexpression of CDK4 partly alleviates the cell growth defect of c-*myc*-deficient cells (Hermeking *et al*, 2002). By contrast, it has also been shown that the overexpression of cyclin D1, E, or A alone does not significantly improve the doubling time of c-*myc*-deficient cells (Mateyak *et al*, 1999). Thus, it is possible that not a single but multiple cell cycle regulators of G1 phase are directly or indirectly activated by ATF3, and these combined effects lead to a significant decrease in doubling time. Consistent with this notion, the expressions of cyclins E and A were strongly upregulated in our microarray analysis (data not shown). We have previously shown that ATF3 downregulates p53 gene transcription (Kawauchi *et al*, 2002), which may result in the downregulation of the cell cycle inhibitor p21. The level of p21, however, was not significantly influenced in c-*myc*-deficient cells by ATF3 (data not shown). It should be noted here that the cell cycle progression of c-*myc*-deficient cells was enhanced only in the presence of serum (Figure 5B). Although it is not clear at this moment why serum signal is required in addition to the ectopic expression of ATF3, we speculate that target gene(s) of ATF3 including cell cycle regulators is controlled in a serum-dependent manner. Nevertheless, partial but significant rescue of proliferation of c-*myc*-deficient cells by ATF3 is noteworthy, since such a remarkable restoration has never been observed by any other target genes of c-Myc. Identification of ATF3 targets, direct or indirect, may uncover the underlying molecular mechanism by which ATF3 controls cell cycle, and such a study is now in progress.

Our study demonstrates for the first time a crosstalk regulation between c-*myc* and *ATF3* in cell proliferation. ATF3 is rapidly induced in the regenerating liver (Hsu *et al*, 1991; Mohn *et al*, 1991), very early in which c-*myc* transcript is also induced (Makino *et al*, 1984). Thus, c-Myc and ATF3 together may regulate liver regeneration. Moreover, ATF3 is overexpressed in murine melanoma cells with high metastatic potentials (Ishiguro *et al*, 1996), and the *ATF3* gene is amplified in esophageal cancer cells (Prmkhaokham *et al*, 2000). Since c-Myc expression is commonly deregulated in hepatocellular cancer with poor prognosis (Shachaf *et al*, 2004), c-Myc/ATF3 crosstalk might play a role in oncogenesis and its progression.

Finally, our results demonstrate for the first time that ATF3 promotes the proliferation of c-*myc*-deficient cells by alleviating their impeded G1-phase progression. This provides a novel functional interaction between the stress response gene *ATF3* and the proto-oncogene c-*myc*. Further investigations should shed light on the biological implications of ATF3 in cellular stress response, cell proliferation, and oncogenesis.

Materials and methods

Reagents

Antibodies used were anti-ATF3 (C-19), anti-c-Myc (N-262), anti-ATF2 (N-96), anti-c-Jun (H-79), anti-cyclin E (M-20), anti-cyclin A

(C-19), anti-CDK4 (C-22), and anti-CDK2 (M2) antibodies from Santa Cruz, anti-c-Myc (R950-25) antibody from Invitrogen, anti-cyclin D1(Ab-3) from Calbiochem, anti-p44/42 MAPK (#9101) and anti-phospho-p44/42 MAP (Thr202/Try204) E10 antibody (#9102) from Cell Signaling Technology, and anti-Flag (F-3165) and anti-β-tubulin (T-4026) antibodies from Sigma. Expression plasmids for c-Myc and LacZ contained mouse c-Myc and LacZ cDNAs, respectively, under the control of the SRα promoter in pcDEBΔ, as described (Nakabeppu *et al*, 1993). PD98059, SP600125, and SB203580 were from Calbiochem and etoposide was from Sigma. Other biochemicals used were reagents grade.

Cell culture and serum treatment

TGR-1 is a subclone of the immortalized rat embryonic Rat-1 cell line. The HO15.19 and HET15 cell lines contain homozygous or heterozygous deletions of the c-*myc* gene, respectively, as described previously (Mateyak *et al*, 1997). HO/myc3 cell line is a c-*myc* transgene-expressing derivative of the HO15.19 cell line (Mateyak *et al*, 1999). Cells were cultured in Dulbecco's modified Eagle's medium supplemented with 10% calf serum, 100 U/ml penicillin, and 100 μg/ml streptomycin in a 5% CO_2 atmosphere at 37°C. For serum stimulation, cells were first starved in medium containing 0.25% serum for 48 h and subsequently stimulated with 10% serum for the indicated times.

RNA isolation and Northern blot analysis

Total RNA (10 μg) was isolated by an acid-guanidinium method and subjected to Northern blot analysis using cDNA probe for the rat ATF3 gene, as described (Cai *et al*, 2000). Rat ATF3 cDNA was a generous gift from Dr T Hai of Ohio University.

Whole-cell extract preparation and Western blot analysis

Whole-cell extract was prepared as described (Kawauchi *et al*, 2002), and the amount of protein was quantitated using bovine serum albumin as a standard (Lowry *et al*, 1951). Whole-cell protein extract (20 μg) was separated on an SDS–polyacrylamide gel, subjected to Western blot analysis, and visualized by chemiluminescence according to the ECL kit protocol from Amersham.

Luciferase assay

Reporter plasmids containing various lengths of the 5′-upstream region of the human ATF3 gene promoter or mutations of ATF/CRE motif at −92 and −85 are as described (Cai *et al*, 2000). Approximately 3×10^5 cells at 70–80% confluency in a 35 mm dish were cotransfected with reporter plasmid and the effector expression vector. After serum starvation in media containing 0.25% serum for 48 h, cells were stimulated with 10% serum and incubated for another 24 h. Serum-starved cells were also treated by 25 μM PD98059 for 2 h, and then stimulated by serum. Supernatants of cell extracts were assayed for firefly and seapansy luciferase activity using a dual luciferase reporter assay system (Promega). pRL-CMV (Toyo Ink) containing the seapansy luciferase gene was used as an internal control for transfection and expression.

Electrophoretic mobility shift assay

Nuclear extracts were prepared from the serum-starved and serum-fed TGR1 cells (2×10^7 cells), as described (Cai *et al*, 2000). Nuclear protein extracts (2 μg) were incubated in 20 μl of binding buffer (10 mM HEPES–KOH, pH 7.9, 60 mM KCl, 0.5 mM EDTA, 5 mM $MgCl_2$, 0.1 mM PMSF, 5 mM β-mercaptoethanol) containing 0.5 μg of poly(dI-dC) and 0.5 ng of radiolabeled DNA probe at room temperature for 30 min. For the supershift assay, 0.1 μg of anti-ATF2, -c-Jun, or -c-Myc antibodies were added and incubated for another 30 min. DNA probe was obtained by annealing 0.1 μg each of sense and antisense oligonucleotides for ATF/CRE site as described previously (Cai *et al*, 2000), and radiolabeled with 25 μCi of [γ-^{32}P]ATP (6000 Ci/mmol) and polynucleotide kinase. Binding mixture was applied onto a 5% nondenaturing polyacrylamide slab gel in Tris–borate–EDTA buffer. After electrophoresis, the gel was dried on a 3 MM Whatman paper and visualized by Fuji Bas 2500 image analyzer.

Chromatin immunoprecipitation assay

ChIP assays were performed according to the protocol supplied from Upstate. Immunoprecipitations were performed using indicated antibodies. PCR was performed with the following primer pairs for three different regions of ATF3 gene promoter: ATF/CRE promoter region from −120 to +30, 5′-GGCCAGTTCTCCCTG GAAGC-3′ and 5′-AAGCACCTGGCACCGCGCGT-3′; upstream region 1 from −370 to −120, 5′-GCCGGTAACCGTGTGGATTC-3′ and 5′-GACTAGGTGAGGCTGGGAAG-3′; and upstream region 2 from −570 to −370, 5′-TAGCGGAGGGAGAGATGCCA-3′ and 5′-GAGACCGCG GACTTGGTGAT-3′.

Binding assay

For *in vivo* binding, 293T cells (3×10^6 cells) were transfected with 3 μg each of expression vectors for c-Myc, ATF2, and c-Jun. At 48 h after transfection, whole-cell extracts were prepared and incubated with 0.5 μg of indicated antibody at 4°C for 3 h, followed by incubating with 30 μl Protein G-Sepharose (Pharmacia) for 2 h. The resulting immunocomplex was washed and subjected to Western blot analysis. For *in vitro* binding, full-length c-Myc was expressed as GST fusion using pGEX-6P1 (Pharmacia), and ATF2 and c-Jun were expressed using pET21a (Novagen). Bacterial extracts containing these recombinant proteins were mixed in a binding buffer (50 mM Tris–HCl, pH 8.0, 0.1 M NaCl, 1 mM EDTA, 1 mM β-mercaptoethanol, 10% glycerol) at 4°C for 60 min. After further incubation with 30 μl of glutathione-Sepharose beads (50% slurry; Pharmacia), or 0.5 μg of anti-ATF2 or anti-c-Jun antibody followed by 30 μl Protein G-Sepharose, protein complex was washed and detected by Western blot using indicated antibody.

Ectopic expression of ATF3 by adenovirus or retrovirus gene transfer

Adenovirus vectors encoding the full-length human ATF3 gene (AdATF3) or β-galactosidase (AdLacZ) were prepared using standard methods (Miyake *et al*, 1996) as described earlier (Kawauchi *et al*, 2002). For preparing retrovirus encoding the human ATF3, 543 bp of cDNA was subcloned into the *Xho*1 site of the retrovirus vector pMXs-neo and packaged in Plat-E cells (Morita *et al*, 2000). Following the infection of c-*myc*-deficient HO15.19 cells, colonies were selected with 400 or 600 μg/ml of G418 (nacalai).

Isolation of TGR1 cell lines stably expressing ATF3 siRNA

Oligonucleotides for expressing stem–loop RNAs that target two different regions of rat ATF3 were subcloned into pMXneo under human U6 promoter. The vector was kindly supplied by Dr T Adachi from our institute. Sequences used were:

#1 5′-GATCGAAGGAACATTGCAGAGCTGTGTGCTGTCCAGCTCTGC AATGTTCCTTCTTTTG-3′ and
5′-GATCCAAAAGAAGGAACATTGCAGAGCTGGACAGCACACAGCTC TGCAATGTTCCTTC-3′, and
#2 5′-GATCGAATGAGAAGCAGCATCTGGTGTGCTGTCCCAGATGCT GCTTCTCATTCTTTTG-3′ and
5′-GATCCAAAAGAATGAGAAGCAGCATCTGGGACAGCACACCAGAT GCTGCTTCTCATTC-3′

that target amino-acid regions from 176 to 181 and from 137 to 142, respectively. Wild-type TGR1 cells were infected with these retroviruses and cultured in media containing 800 μg/ml of G418.

Assay for serum-induced cell proliferation

Cells treated as indicated were starved in medium containing 0.25% serum. After 48 h, cells were stimulated with 10% serum and cell number was measured at the indicated time intervals. By staining with 0.2% Trypan blue, cell viability was more than 95% in all assays.

Fluorescence-activated cell sorting analysis

Approximately 3×10^5 asynchronously cycling cells were harvested, washed once with PBS, and fixed with 70% ice-cold ethanol. After staining with 50 μg/ml of propidium iodide, DNA content of the cells was analyzed by using FACScan (Becton Dickinson). Cells at each phase of the cell cycle were measured and expressed as percent of total cells.

BrdU incorporation assay

Asynchronously cycling cells were pulse-labeled by BrdU for 15 min using *in situ* cell proliferation kit (Roche) and its incorporation value was determined by scoring BrdU-positive cells after histochemical staining as described (Schorl and Sedivy, 2003). Cells

(1×10^4 cells) were also synchronized in M phase by mitotic shake-off, plated in 24-well plates, and labeled by 10 μM BrdU. At each time point indicated, BrdU incorporation was stopped by adding ascorbic acid to a final concentration of 67 mM, and the labeled cells were counted after staining with anti-BrdU monoclonal antibody from Roche. Percent of BrdU-positive cells was scored as labeling index (Schorl and Sedivy, 2003).

Statistical analysis

Multiple comparisons were evaluated by ANOVA followed by Scheffe's *post hoc* test. Data are presented as mean ± s.d. Statistical significance was assigned at the level of $P<0.05$.

Supplementary data

Supplementary data are available at *The EMBO Journal* Online.

Acknowledgements

We thank Dr T Hai at Ohio, USA for her generous gift of rat ATF3 cDNA and Dr S Yokoi from our institute for her technical advice for ChIP assay. This work was supported in part by a Grant-in-Aid for Scientific Research from the Ministry of Education, Science, Sports, Culture and Technology of Japan, the Japan Society for the Promotion of Science. IG and JMS were supported in part by NIH grant GM41690 to JMS.

References

Allan AL, Albanese C, Pestell RG., LaMarre J (2001) Activating transcription factor 3 induces DNA synthesis and expression of cyclin D1 in hepatocytes. *J Biol Chem* **276:** 27272–27280

Cai Y, Zhang C, Nawa T, Aso T, Tanaka M, Oshiro S, Ichijo H, Kitajima S (2000) Homocysteine-responsive ATF3 gene expression in human vascular endothelial cells: activation of c-Jun NH_2 terminal kinase and promoter response element. *Blood* **96:** 2140–2148

Cheng SW, Davies KP, Yung E, Beltran RJ, Yu J, Kalpana GV (1999) c-Myc interacts with INI1/hSNF5 and requires the SWI/SNF complex for transactivation function. *Nat Genet* **22:** 102–105

Davis AC, Wims M, Spotts GD, Hann SR, Bradley A (1993) A null c-*myc* mutation caused lethality before 10.5 days of gestation in homozygotes and reduced fertility in heterozygous female mice. *Genes Dev* **7:** 671–682

de Alboran IM, O'Hagan RC, Gartner F, Malynn B, Davidson L, Rickert R, Rajewsky K, DePinho RA, Alt FW (2001) Analysis of c-Myc function in normal cells via conditional gene-targeted mutation. *Immunity* **14:** 45–55

de Ruiter ND, Wolthuis RMF, van Dam H, Burgering BMT, Bos JL (2000) Ras-dependent regulation of c-Jun phosphorylation is mediated by the Ral guanine nucleotide exchange factor–Ral pathway. *Mol Cell Biol* **20:** 8480–8488

Eberhardy SR, Farnham PJ (2001) c-Myc mediates activation of the cad promoter via a post-RNA polymerase II recruitment mechanism. *J Biol Chem* **276:** 48562–48571

Fan F, Jin S, Amundson SA, Tong T, Fan W, Zhao H, Zhu X, Mazzacurati L, Li X, Petrik KL, Fornace AJ, Rajasekaran B, Zhan Q (2002) ATF3 induction following DNA damage is regulated by distinct signaling pathways and over-expression of ATF3 protein suppresses cell growth. *Oncogene* **21:** 7488–7496

Fernandez PC, Frank SR, Wang L, Schroeder M, Liu S, Greene J, Cocito A, Amati B (2003) Genomic targets of the human c-Myc protein. *Genes Dev* **17:** 1115–1129

Hai T, Wolfgang CD, Marsee DK, Allen AE, Sivaprasad U (1999) ATF3 and stress responses. *Gene Expression* **7:** 321–335

Henriksson M, Luscher B (1996) Proteins of the Myc network. Essential regulators of cell growth and differentiation. *Adv Cancer Res* **68:** 109–182

Hermeking H, Rago C, Schuhmacher M, Li Q, Barrett JF, Obaya AJ, O'Connell BC, Mateyak MK, Tam W, Kohlhuber F, Dang CV, Sedivy JM, Erick D, Vogelstein B, Kinzler KW (2002) Identification of CDK4 as a target of c-Myc. *Proc Natl Acad Sci USA* **97:** 2229–2234

Hsu JC, Laz T, Mohn KL, Taub R (1991) Identification of LRF-1, a leucine-zipper protein that is rapidly and highly induced in regenerating liver. *Proc Natl Acad Sci USA* **88:** 3511–3515

Inoue K, Zama T, Kamimotto T, Aoki R, Ikeda Y, Kimura H, Hagiwara M (2004) TNFα-induced ATF3 expression is bidirectionally regulated by the JNK and ERK pathway in vascular endothelial cells. *Genes Cells* **9:** 59–70

Ishiguro T, Nakajima M, Naito M, Muto T, Tsuruo T (1996) Identification of genes differentially expressed in B6 murine melanoma sublines with different metastatic potentials. *Cancer Res* **56:** 875–879

Iyer VR, Eisen MB, Ross DT, Schuler G., Moore T, Lee JCF, Trent JM, Staudt LM, Hudson J, Boguski MS, Lashkari D, Shalon D, Botstein D, Brown PO (1999) The transcriptional program in the response of human fibroblasts to serum. *Science* **283:** 83–87

Kang Y, Chen CR, Massague J (2003) A self-enabling TGFβ response coupled to stress signaling: Smad engages stress response factor ATF3 for Id1 repression in epithelial cells. *Mol Cell* **11:** 915–926

Kawauchi J, Zhang C, Nobori K, Hashimoto Y, Adachi TM, Noda A, Sunamori M, Kitajima S (2002) Transcriptional repressor activating transcription factor 3 protects human umbilical vein endothelial cells from tumor necrosis factor-alpha-induced apoptosis through down-regulation of p53 transcription. *J Biol Chem* **277:** 39025–39034

Liang G, Wolfgang CD, Chen BPC, Chen TH, Hai T (1996) ATF3 gene. Genomic organization, promoter, and regulation. *J Biol Chem* **271:** 1695–1701

Lowry OH, Rosebrough NJ, Farr AL, Randall RJ (1951) Protein measurement with the folin phenol reagent. *J Biol Chem* **193:** 265–275

Makino R, Hayashi K, Sugimura T (1984) c-*myc* transcript is induced in rat liver at a very early stage of regeneration or by cycloheximide treatment. *Nature* **310:** 697–698

Mateyak MK, Obaya AJ, Adachi S, Sedivy JM (1997) Phenotypes of c-Myc-deficient rat fibroblasts isolated by targeted homologous recombination. *Cell Growth Differ* **8:** 1039–1048

Mateyak MK, Obaya AJ, Sedivy JM (1999) c-Myc regulates cyclin D-cdk4 and -cdk6 activity but affects cell cycle progression at multiple independent points. *Mol Cell Biol* **19:** 4672–4683

McMahon SB, Wood MA, Cole MD (2000) The essential cofactor TRRAP recruits the histone acetyltransferase hGCN5 to c-Myc. *Mol Cell Biol* **20:** 556–562

Menssen A, Hermeking H (2002) Characterization of the c-Myc-regulated transcriptome by SAGE: identification and analysis of c-Myc target genes. *Proc Natl Acad Sci USA* **99:** 6247–6279

Miyake S, Kanegae Y, Harada S, Sato Y, Takamori K, Tokuda C, Saito I (1996) Efficient generation of recombinant adenoviruses using adenovirus DNA-terminal protein complex and a cosmid bearing the full-length virus genome. *Proc Natl Acad Sci USA* **93:** 1320–1324

Mohn KL, Laz TM, Hsu JC, Melby AE, Bravo R, Taub R (1991) The immediate-early growth response in regenerating liver and insulin-stimulated H-35 cells: comparison with serum-stimulated 3T3 cells and identification of 41 novel immediate-early genes. *Mol Cell Biol* **11:** 381–390

Morita S, Kojima T, Kitamura T (2000) Plat-E: an efficient and stable system for transient packaging of retroviruses. *Gene Therapy* **7:** 1063–1066

Nakabeppu Y, Oda S, Sekiguichi M (1993) Proliferative activation of quiescent Rat-1A cells by ΔFosB. *Mol Cell Biol* **13:** 4157–4166

Nakagomi S, Suzuki Y, Namikawa K, Kiryu-Seo S, Kiyama H (2003) Expression of the activating transcription factor ATF3 prevents c-Jun N-terminal kinase-induced neuronal death by promoting heat shock protein 27 expression and akt activation. *J Neurochem* **23:** 5187–5196

Nobori K, Ito H, Adachi TM, Adachi S, Ono Y, Kawauchi J, Kitajima S, Marumo F, Isobe M (2002) ATF3 inhibits doxorubicin-induced apoptosis in cardiac myocytes: a novel cardioprotective role of ATF3. *J Mol Cell Cardiol* **34:** 1387–1397

O'Connell BC, Cheung AF, Simkevich CP, Tam W, Ren X, Mateyak MK, Sedivy JM (2003) A large scale genetic analysis of c-Myc-regulated gene expression patterns. *J Biol Chem* **278:** 12563–12573